X-RAY TIMING PROPERTIES OF FOUR ANOMALOUS X-RAY PULSARS: 4U 0142+61, 1E 2259+586, 1RXS J170849.0–400910, AND 1E 1841–045

A THESIS SUBMITTED TO
THE GRADUATE SCHOOL OF NATURAL AND APPLIED SCIENCES
OF
MIDDLE EAST TECHNICAL UNIVERSITY

BY

DANJELA ÇERRI

IN PARTIAL FULFILLMENT OF THE REQUIREMENTS
FOR
THE DEGREE OF MASTER OF SCIENCE
IN
PHYSICS

JANUARY 2015

Approval of the thesis:

X-RAY TIMING PROPERTIES OF FOUR ANOMALOUS X-RAY PULSARS: 4U 0142+61, 1E 2259+586, 1RXS J170849.0–400910, AND 1E 1841–045

submitted by **DANJELA ÇERRI** in partial fulfillment of the requirements for the degree of **Master of Science in Physics Department, Middle East Technical University** by,

Prof. Dr. Gübin Dural Ünver _____
Dean, Graduate School of **Natural and Applied Sciences**

Prof. Dr. Mehmet T. Zeyrek _____
Head of Department, **Physics**

Prof. Dr. Altan Baykal _____
Supervisor, **Physics Department, METU**

Assoc. Prof. Dr. Sıtkı Çağdaş İnam _____
Co-supervisor, **EE Eng. Dept., Başkent Uni.**

Examining Committee Members:

Prof. Dr. Sacit Özdemir
Astronomy and Space Sciences Dept, Ankara Uni. _____

Prof. Dr. Altan Baykal
Physics Department, METU _____

Assoc. Prof. Dr. Sıtkı Çağdaş İnam
Electrical and Electronics Eng. Dept., Başkent Uni. _____

Prof. Dr. Ümit Kızıloğlu
Physics Department, METU _____

Assoc. Prof. Dr. Sinan Kaan Yerli
Physics Department, METU _____

Date: _____

I hereby declare that all information in this document has been obtained and presented in accordance with academic rules and ethical conduct. I also declare that, as required by these rules and conduct, I have fully cited and referenced all material and results that are not original to this work.

Name, Last Name: DANJELA ÇERRI

Signature :

ABSTRACT

X-RAY TIMING PROPERTIES OF FOUR ANOMALOUS X-RAY PULSARS: 4U 0142+61, 1E 2259+586, 1RXS J170849.0–400910, AND 1E 1841–045

Çerri, Danjela

M.S., Department of Physics

Supervisor : Prof. Dr. Altan Baykal

Co-Supervisor : Assoc. Prof. Dr. Sıtkı Çağdaş İnam

January 2015, 65 pages

In this thesis, the detailed X-ray timing characteristics of four Anomalous X-Ray Pulsars (AXPs); 4U 0142+61, 1E 2259+586, 1RXS J170849.0–400910, and 1E 1841–045 are presented for glitch free time intervals using data taken by *Rossi X-Ray Timing Explorer (RXTE)*. The pulse arrival times of these AXPs are evaluated by phase coherent timing method. After the removal of the spin-down trend from pulse arrivals, remaining residuals are used for estimation of their noise strengths. Possible correlation of the noise strength with spin-down rate is investigated for individual sources in different time intervals, for AXP class and for whole magnetars. Our initial results indicate that noise strength of these objects are scaling up with their spin down rates for AXPs and magnetars.

Keywords: Magnetars, Anomalous X-Ray Pulsars, Timing Noise

ÖZ

4U 0142+61, 1E 2259+586, 1RXS J170849.0–400910 VE 1E 1841–045
ANORMAL X-IŞINI ATARCALARININ X-IŞINI ZAMANLAMA
ÖZELLİKLERİ

Çerri, Danjela

Yüksek Lisans, Fizik Bölümü

Tez Yöneticisi : Prof. Dr. Altan Baykal

Ortak Tez Yöneticisi : Assoc. Prof. Dr. Sıtkı Çağdaş İnam

Ocak 2015 , 65 sayfa

Bu tezde, Anormal X-Işını Atarcaları (AXP) 4U 0142+61, 1E 2259+586, 1RXS J170849.0-400910, ve 1E 1841-045 için periyot kayması olmayan zaman aralıkları kullanılarak *Rossi X-Ray Timing Exporer (RXTE)* verileri ile elde edilen detaylı X-Işını zamanlama özellikleri sunulmaktadır. Bu AXP kaynakları için atım geliş zamanları, faz-tutarlı zamanlama methodu kullanılarak hesaplanmıştır. Elde edilen atım geliş zamanlarından, kaynakların atım frekansı yavaşlama oranı modellenerek cıkarılmış ve bu şekilde zamanlama artıkları elde edilmiştir. Bu zamanlama artıkları ise zamanlama gürültüsü gücünün hesaplanmasında kullanılmıştır. Zamanlama gürültüsü gücünün atım frekansı yavaşlama oranı ile muhtemel bağıntıları üç farklı durum için: 1) farklı zaman aralıklarında aynı kaynak için, 2) Anormal X-Işını Atarcaları sınıfı için, ve 3) bütün magnetar kaynakları için araştırılmıştır. Elde edilen sonuçlar AXP kaynakları için zaman-

lama gürültüsü gücünü atım frekansı yavaşlama oranı ile ilişkili olarak arttığını göstermektedir.

Anahtar Kelimeler: Magnetarlar, Anormal X-Işını Atarcaları, Zamanlama Gürültüsü

to my family and my fiance

ACKNOWLEDGEMENTS

I own my gratitude to my supervisor Prof. Dr. Altan Baykal for his concern, guidance and encouragement throughout my master studies. Thanks to him I was able to follow my master degree studies. I also would like to thank my co-advisor Assoc. Prof. Dr. Sıtkı Çağdaş İnam and the committee members: Prof. Ümit Kızıloğlu, Assoc. Prof. Dr. Sinan Kaan Yerli and in particular Prof. Sacit Özdemir for their valuable reviews of the thesis.

I dedicate this thesis to my colleague and friend who later became my fiancé M. Miraç Serim. It was his tireless help and support that made me reach these days: graduate and gain my self-esteem again. I can undoubtedly say that I could not have made it if he was not there to patiently listen all the problems I had, and find a solution so I could smile again. I am so thankful to have had him around.

Throughout my life, the love and support of my family has been my solid motivation to carry on. I am indebted to them, especially to my brother Besart Çerri for making the impossible to ease my work and follow my dream of studying astrophysics. I also would like to thank Arjete Brahusha, Bebeta Hoxha, Anastasia Çeka, Estela Zani, Arjola Balilaj, Adlira Hadroj, Edona Fasllija, Festa Buçinca, Erald Varaku and all my Albanian friends for being like a family to me throughout my life in Turkey. In addition, I also thank my colleagues Şeyda Şahiner and Dr. Suat Dengiz for their time and useful discussions while writing the thesis.

I acknowledge TÜBİTAK (The Scientific and Technological Research Council of TURKEY) for supporting this study with the project 109T748 during my master study.

TABLE OF CONTENTS

LIST OF TABLES

TABLES

LIST OF FIGURES

FIGURES

CHAPTER 1

INTRODUCTION

In this chapter, the observational properties of Anomalous X-ray Pulsars (AXPs) and Soft Gamma Repeaters (SGRs) will be presented as well as their historical background.

1.1 Introduction

It is commonly accepted that a core collapse supernova of an intermediate-massive star (8-25 solar mass) generally results in the formation of a compact object, mostly composed of neutrons, which we call it a neutron star. The possible existence of neutron stars was firstly proposed by [5]. They claimed that a core-collapse supernova of an intermediate mass star could result in ultra-dense object composed of neutrons. Since then, several attempts to explain and discover such objects were made; however, science had to wait until in 1967 to take the first pulses from a neutron star [42]. From then on a lot of great discoveries were made related to these exotic objects. So far we know that neutron stars are ultra-dense compact objects mostly formed from core-collapse supernova. Their typical radii and masses are $\sim$ 10 km and $\sim$ 1.4 solar mass, respectively [61]. Such values of volume and mass lead to an average density of $\sim 10^{13} - 10^{14} g/cm^3$ and only neutron degeneracy pressure can hold the star from further collapsing by gravitational pressure. The exact composition of neuron star's interior is not known yet; however it is thought to be composed of several layers.

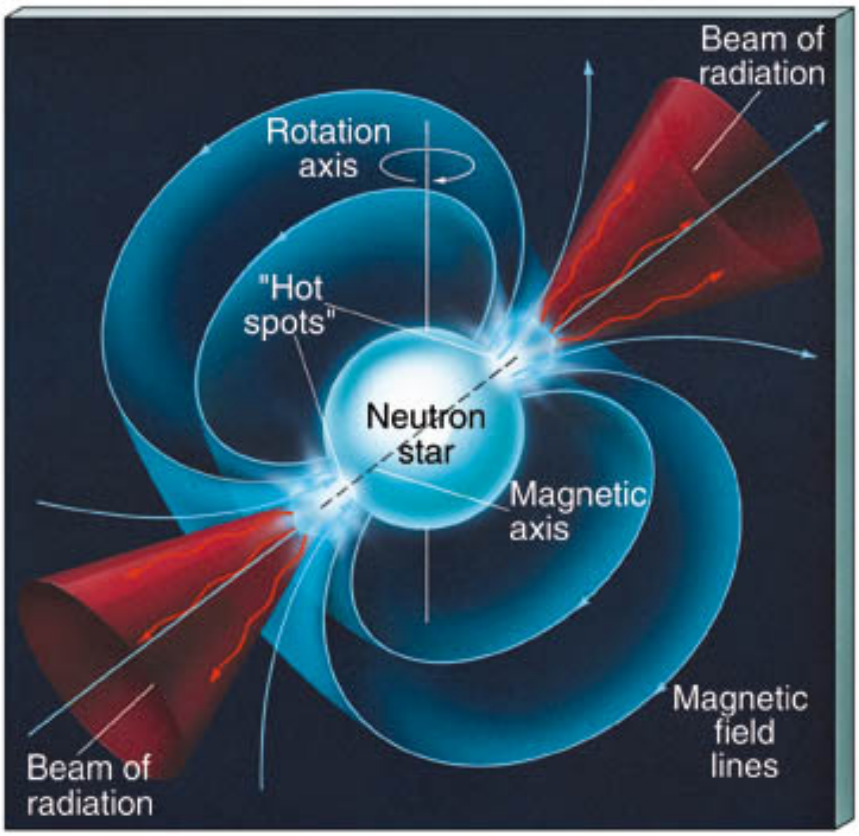

Figure 1.1: A sample pulsar figure showing oblique magnetic field and emission region[1]

When young, most of neutron stars host a typical external magnetic field of B$\sim 10^{11} - 10^{12}$ G [9]. When the rotational axis is different from the magnetic field axis (see figure 1.1), the beams coming from magnetic poles of these sources are detected as pulses, provided the line of sight sweeps the Earth. Neutron stars which have magnetic field strengths of the order of B$\sim 10^{11} - 10^{12}$ G and emit electromagnetic waves in the direction of Earth are called pulsars.

Pulsars are classified in two main groups according to their emission power: rotation powered pulsars and accretion powered pulsars. Rotation powered pulsars gain their energy by the process called magnetic braking in which the loss of rotational kinetic energy is converted into emission energy. While the accretion powered pulsars gain their energy from the loss of gravitational potential energy of the accreting matter. In some special circumstances the magnetic field of a pulsar can get up to $\sim 10^{16}$ G. Such highly magnetized objects are called mag-

[1]Figure 1.1 Taken from Astronomy Today 6th edition Chaisson and McMillan(2007)

netars. The emission mechanism is different from the vast majority of pulsars and it is thought to be powered by the decay of magnetic field. Magnetars are divided into two groups Anomalous X-ray Pulsars (AXPs) and Soft Gamma-ray Repeaters (SGRs). This thesis will consist of detailed investigation of timing parameters of four magnetars.

1.2 Overview of Magnetars

The first emission observed from a magnetar was in January 7, 1979 from the so called SGR 1806–20. It was a short (0.1s) burst of gamma rays with the peak luminosity of $\sim 10^{41}$ erg/s [63]. Because the burst was in gamma ray energy band, it was classified as a Gamma Ray Burst(GRB) event, even though there were some differences of this burst compared to the classical GRBs. A GRB is a very energetic collapse of an extremely big star exploding in a supernova called a hypernova [72];[43], it is a one-time event and its energy is spread uniformly into space. Around two months later, on March 5, 1979, another gamma ray burst was detected, the intensity of which went beyond the capacity of the detectors [31]. This burst had a 0.2 seconds flare, a slow decay of 8 s and a peak luminosity of 10^{45} erg/s; furthermore, it was located in Large Magellanic Cloud (LMC) and was associated with the supernova remnant N49 [64]. This source is now known as SGR 0526–66. On the very next day, on March 6, 1979, another burst with 1.5s duration was detected and about 30 days later the same source released two more burst. As mentioned above, GRBs are one-time events i.e. we can not see more than one GRB from the same source. The fact that the bursts observed are repetitive and the spectra of the bursts were softer than the spectra of GRBs led astrophysicist call this class of objects Soft Gamma-ray Repeaters (SGRs). The models proposed in the first years of the discovery of SGRs were unable to explain both, the giant flares and the repeatedly occurring bursts. For this reason the physics behind the SGRs was blurry for several years. The proposal of magnetar model [27] changed the course of events related with SGRs. According to this model SGRs are young neutron stars with an enormous magnetic fields (100-1000 times higher than normal pulsars which have magnetic

fields of the order $\sim 10^{12}$ G); these sources have persistent X-ray emission, and they are powered by the decay of the magnetic field. Magnetic dipole braking is the reason of SGR spin-down [27]; [71]; [81]; [82] (A detailed explanation of magnetar model is found in section 2.1.1). The mechanism explained in this model encountered some doubts until it was proved by observational evidence. The discovery of the persistent X-ray emission with a period of 7.5s from SGR 1806–20, and the discovery of its spin-down rate (which was relatively rapid) was very important because the magnetic field implied from these values was proving (independently from SGR bursts) that magnetic field strength is of the orders $\sim 10^{15}$ G, a lot higher than the value of canonical pulsars [56].

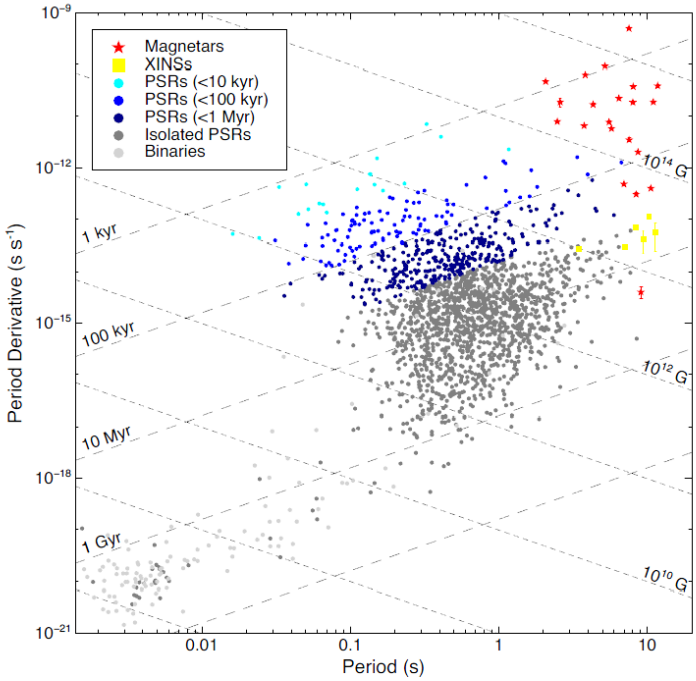

Figure 1.2: Distribution of pulsars regarding their spin period (x-axis) and the spin down rate (y-axis)[2], grey dots indicate binaries, darker grey dots indicate isolated pulsars, black, blue, and refers to pulsars with different age groups, yellow squares indicate X-Ray isolated neutron stars and red stars indicate magnetar sources.

Along with the discovery of SGRs, a group of cosmological sources called Anomalous X-ray Pulsars (AXPs) were being discovered simultaneously. The first emission from an AXP was detected on 1981 from 1E 2259+586 [32]. At first,

[2]Taken from [70]

the source was classified as a Low Mass X-ray Binary because the IR/Optical observations excluded the possibility of being a High-Mass X-ray Binary. 1E 2259+586 is located in the center of the supernova CTB 109. This fact made Fahlman and Gregory [32] be suspicious about the classification because, if everything was as it seemed, this 'binary system' would be the first of its kind to be located inside a supernova remnant. A few years later 1E 1048.1–5937 [79] and 4U 0142+61 [49] were discovered. The inconsistencies like no evidence of a massive companions, location inside a supernova remnant, no evidence of orbital modulation among others, led Mereghetti and Stella [67] suggest that these sources are LMXBs with very very low mass companions. van Paradijs et al. [88] called these sources 'Anomalous X-ray Pulsars' regarding the fact that they were anomalous compared to the classical ones (pulsars). Since then, several sources that have similar characteristic like spin period, spin-down rate, luminosities, spectral properties are identified and classified as Anomalous X-ray Pulsars. Like SGRs, magnetar model is also valid for AXPs according to Thompson and Duncan [82]. They proposed that AXPs are ultra-magnetized, young neutron stars which are powered by the decay of the magnetic field.

Several years after their discovery, SGRs and AXPs had been treated as two distinct groups of neutron stars. Basically, SGRs were sources that burst and had flares while AXPs were spin-down sources with persistent X-ray emission. The distinction became blurry when two AXPs were observed to have SGR-like bursts [37]; [53]. So far both groups share the same characteristics; i.e. AXPs show bursting behavior as in SGRs, meanwhile SGRs show AXP-like behaviors like spin-down and persistent X-ray emission in their quiescent phase [51]. Recently, Olausen and Kaspi [70] claimed that AXPs and SGRs are sources of the same class, widely identified as magnetars.

Magnetars are neutron stars with spin periods (P) clustering in the narrow range of 2-12s and spin-down rates ($\dot{P}$ of $10^{-13} - 10^{-11}$ s/s ([94]; [65]), hence they occupy the very upper right part of $P - \dot{P}$ diagram (see figure 1.2) These values imply a magnetic field of B$\sim 10^{13} - 10^{15}$ G. The inferred age of AXPs and SGRs from the spin period and spin-down rate is 10-100kyr, showing that these sources are young neutron stars. Other independent proofs for estimated ages

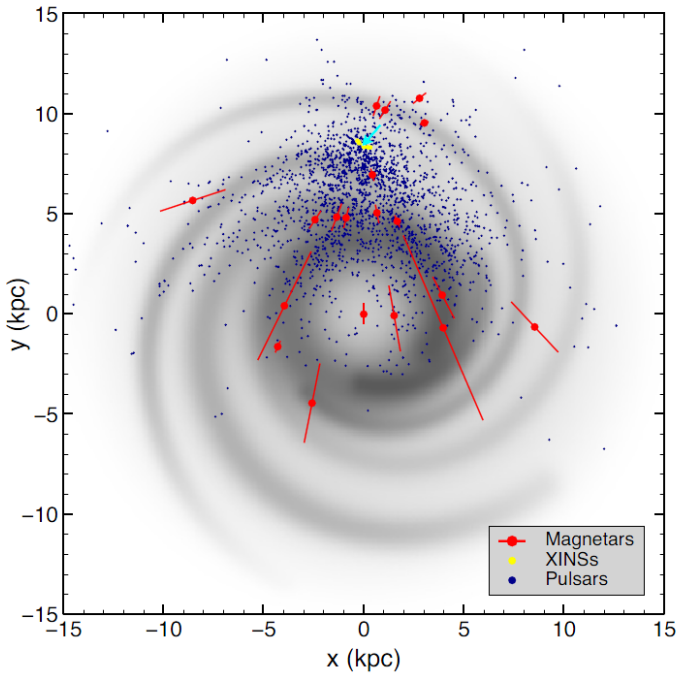

Figure 1.3: Positions of known pulsars in galactic plane of Milky Way[3]Blue, yellow and red dots indicate pulsars, X-ray isolated neutron stars and magnetars, respectively.

are; most of the magnetars reside in the galactic plane (active star formation region, see figure 1.3), and they are associated with supernova remnants [70].

The X-ray luminosities of the magnetars are at the order of $L_x \sim 10^{34} - 10^{36}$ ergs/s. Such high luminosities imply that magnetars are not rotation powered stars. AXPs/SGRs are seen both in soft ($<$ 10keV) and hard ($>$20keV) X-ray band. The soft X-ray spectra can generally be fitted with a steep power law with photon index ranging from $\Gamma \sim 2 - 4$ and a blackbody temperature of $kT \sim 0.5$ [65]. A difference between AXPs and SGRs is that the X-ray spectra of AXPs are usually fitted by both a power-law and a blackbody, while the X-ray spectra of SGRs are fitted by either a power law or a blackbody. The hard X-ray spectra of magnetars is fitted by a flat power-law with photon index values of $\Gamma \sim 0.5 - 1.5$. In addition, magnetars are observed to radiate emission in other wavelengths such as, radio, IR, optical and soft gamma energy band. Up to date there are 26 magnetars known (21 confirmed and 5 candidates, [70]).

[3]Adapted from [70]

This study is aimed towards the understanding of timing characteristics of magnetars. In particular, timing noise of four AXPs will be investigated with a purpose of searching for a correlation with other physical parameters. It is previously claimed that spin down rate might correlate with timing noise strength [78]. In this thesis, the spin-down rate vs. timing noise strength correlation is considered for 3 different cases;

case i: For an individual AXP within different time intervals (i.e. for different spin down rate epochs)

case ii: For different AXPs including different epochs

case iii: For whole magnetar class including SGRs and AXPs

CHAPTER 2

PHYSICAL MODELS AND SELECTED AXPS

In this chapter, the literature on the selected Anomalous X-ray Pulsar will be reviewed. There are several models which are put forward to explain the observational properties of these objects. Among several models, two mostly widely accepted models, namely magnetar model and fall back disk model, will be discussed.

2.1 Physical Models

2.1.1 Magnetar Model[1]

Magnetar Model is a model which explains the properties of magnetars and the mechanism they are generated from. It was firstly proposed by Duncan and Thompson [27] as an attempt to explain the giant flares and burst of SGRs. Since 1992 several papers are published by these authors, and to date it is the most commonly accepted mechanism which explains the nature of SGRs and AXPs.

In this model SGRs and AXPs are young neutron stars with ultra-high magnetic fields ($10^{14} - 10^{15}$ G) and this magnetic field is responsible for the emission of magnetars. The origin of such high magnetic field strengths is not yet completely understood; however, according to magnetar model, a combination of dynamo

[1]Unless cited, material in this section is taken from internet in a page titled 'Magnetars', Soft Gamma Repeaters & Very Strong Magnetic Field written by Robert C. Duncan, http://solomon.as.utexas.edu/magnetar.html.

action with a fast rotational speed of the star immediately after supernova explosion would lead to such high magnetic field strengths [26].

The process how magnetic field is generated is as follows: Neutron stars are very hot when they are first formed and this heat is carried out by convection. Together with neutrons, the star's interior also contain some free charged particles which make the fluid inside the star a very good electrical conductor. While the convection process goes on, some of the magnetic field lines are swept in the fluid and are trapped in because of the conducting nature of the fluid [26]. If the rotational speed of the star is fast enough, the magnetic field lines will be dragged through the star with the help of combined convective and rotational effects via a process called dynamo action. Basically dynamo theory explains how magnetic field is maintained inside the celestial bodies. The criteria for this dynamo action to work is that the convective overturn time is bigger than the rotational period, P. When this criteria is satisfied, a magnetic field up to 10^{16} G can be generated in only first 10 seconds of neutron star formation [26]. After those seconds the star cools down, the dynamo action cease and the magnetic field will be trapped inside the star [82]. The reason why most of the neutron stars do not host such high magnetic field strengths is because the rotational speed is not high enough in the first seconds after their birth.

According to magnetar model, the internal magnetic field strength of the stars is assumed to be stronger than the external magnetic field strength up to a factor of ~ 10, and that the internal field is wound up tightly [83]. The internal field wants to get rearranged in order to be more relaxed and for this reason it pushes the crust from inside. This 'push' is in the shearing form and is responsible for the twisting of the magnetosphere. Appearance of such twisting regions will yield the observed SGR flares(see figure 2.1).

Inside this twisted magnetosphere a current I will be generated. This current will make the charged particles go on the foot-points of the star and hitting it up, thus generating X-ray photons. While going to the foot-points, electrons may collide with the X-ray photons and give them energy via inverse Compton effect. The energetic photons generated through this process are thought to be

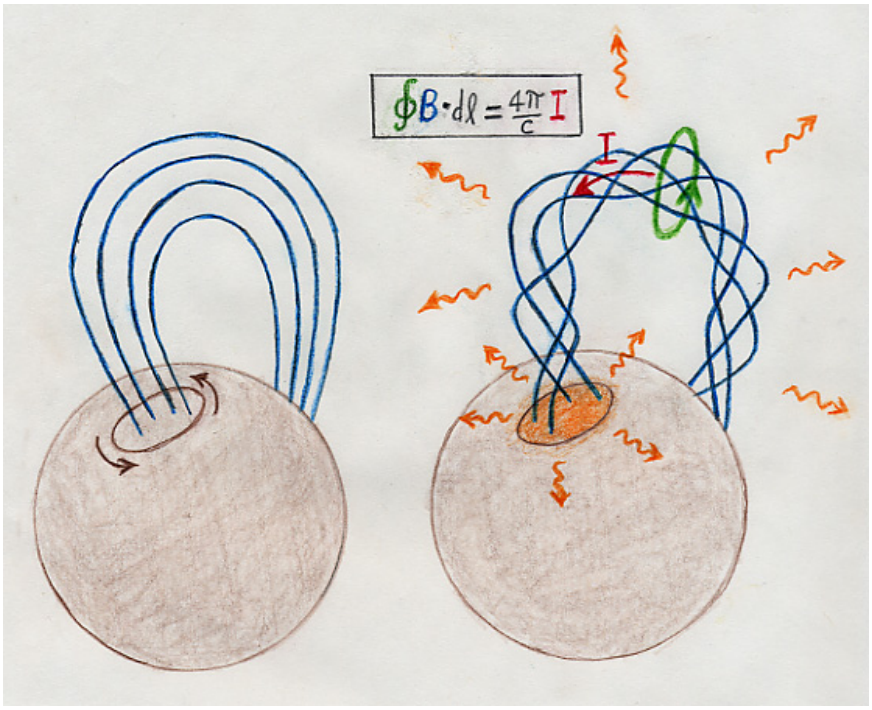

Figure 2.1: The initial magnetic field lines on the surface of magnetar (on the left)is getting twisted as the star rotates (on the right)[2]. The charged particles carried through these lines will be the source of X-ray emission

responsible for the noticeable tail seen in the X-ray spectra of the magnetars.

Magnetar model is widely accepted because it can explain the bursts and flares detected from both AXPs and SGRs. According to this model, sometimes magnetic force of the internal magnetic field is so strong that it locally 'breaks' the crust. When this happens, strong currents outflow in the magnetosphere and we detect them as bursts and flares. Furthermore, magnetic reconfiguration of the magnetosphere and the dissipation of the localized currents also are an origin of the detected bursts and flares.

In magnetar model, the interior of a magnetar is the same as the interior of the neutron stars with the only difference, that is for magnetars there is a very strong wound-up magnetic field due to the fast initial rotation [83]. What magnetar model can not predict is the origin of the IR and optical emission observed for some sources (i.e. AXP 4U 0142+61 [91]).

[2]taken from http://solomon.as.utexas.edu/magnetar.html

2.1.2 Fall Back Disk Model

Another model that attempts to explain the properties of the magnetars is the fallback disk model ([15]; [1]). In principle this model consists of a fossil disk around the magnetar that has remained from the explosion of the progenitor star in a supernova [15]. Alpar [1] suggested that, the evolution of a newborn neutron star could follow a different path of its subsequent evolution (forming a new class of neutron stars, we now call them magnetars), if a third initial condition parameter was added to the first two conditions (which are initial spin period P_0 and magnetic dipole moment μ_{dipole}). This third condition is the existence of a fallback disk of which initial conditions are initial mass and angular momentum of the disk material. The movements of the disk material around a neutron star resemble those of a gyrostat, with an equilibrium period of

$$P_{eq} = \mu^{6/7}(\frac{dM}{dt})^{-3/7}(GM)^{-3/14} \tag{2.1}$$

where P_{eq} is equilibrium period, μ is dipole moment, M is mass of the star and G is the universal gravitational constant. Accretion of matter starts once the disk penetrates inside the Alfven radius. The Alfven radius is a radius where the pressure of the incoming material is equal to magnetic pressure. This accretion is responsible for the X-ray emission of the source. Furthermore, when co-rotation radius r_{co} is smaller than the Alfven radius r_A, disk is in a 'propeller' mode, and, as the matter is propelled, the neutron star transfers angular momentum to the disk material. The loss of the angular momentum causes the neutron star to spin down. The torque of the disk is related to the observed spin-down rates such that

$$I\frac{d\omega}{dt} \sim \mu^2 r_A^{-3} \tag{2.2}$$

where I is the moment of inertia, $\frac{d\omega}{dt}$ is spin down rate.

Those values correspond to a dipole magnetic field of B $\sim 10^{12} - 10^{13}$ G. A fact to notice is that the magnetic field estimated by the fallback disk model is almost ~ 2 orders of magnitude lower than the magnetic field estimated by the magnetar model.

According to fall-back disk model the period clustering exists because the active

time of the disk is limited [2]. Active time depends on the disk properties and the interaction of the disk with the neutron star. After this 'lifetime' the inner radius of the fall back disk r_{in} get back to the edge of the light cylinder radius r_{lc} (i.e. $r_{lc} \sim r_{in}$) and at this stage the luminosity and the energy dissipation drops drastically. At the last stage, the disk becomes passive because the matter cools.

Fallback disk explains the evolution of magnetars. Evidences like **(i)** the emission of 4U 0142+61 in optical/IR band [91], **(ii)** the low magnetic field of SGR 0418+5729 [73], **(iii)** the anomalous braking index and the high magnetic field of PSR J1734-3333 [30] are some of the examples which are explained with the fallback disk model. These examples show that the surface dipole magnetic field may not be the dominant parameter of the total magnetic field of any source (i.e. the total magnetic field may be much higher than the dipole field) [2].

The biggest disadvantage of the fall-back disk model is that it cannot account for the bursts and the flares of SGRs and AXPs. Because in order to produce a SGR flare, the existence of a very strong magnetic field (with the orders of $10^{14}G$) is required.

2.2 Selected Sources

2.2.1 4U 0142+61

AXP 4U 0142+61 is a magnetar at an approximate distance of 3.6kpc [28]). This source was discovered in 1978 with *Uhuru* satellite [34] and it is found in the constellation Cassiopeia. The pulse period of this source is 8.7 s and the period derivative is 0.20×10^{-11} s/s [23]. The P and $\dot{P}$ values implies a dipole magnetic field strength of 1.3×10^{14} G and 4U 0142+61 is the brightest known magnetar to date with a persistent luminosity of $L_x \sim 10^{35}$ erg/s (2-10 keV).

The behavior of AXP 4U 0142+61 is studied in several time intervals divided depending on its timing activities. The initial *RXTE* observations of this source were analyzed by Gavriil and Kaspi [36], and the source was highly stable.

The monitoring of 4U 0142+61 with *RXTE* has been continuous from the first signals to the end of this satellite mission with an exception of only two years (1998-2000).

Until 2006, no outbursts or flares were reported for this source. On 2006 March, 4U 0142+61 started having changes in the pulse morphology that could not be neglected and this was the time when the source entered in an active phase. The active phase lasted for more than one year and during this phase 6 bursts occurred [35]. The duration of the bursts were ranging from 0.4 – 1800 s. Although there was a frequency jump of approximately $1.9 \pm 0.4 \times 10^{-7}$ Hz (which faded away within 17 ± 2 days), 4U 0142+61 had a net spin-down during its active phase of 2006-2007 [35]. This frequency jump is rather called a glitch candidate because its epoch is based only on one time of arrival (TOA) [23]. In 2009 another timing discontinuity (micro-glitch) with a frequency jump of $\Delta\nu = 1.3(2) \times 10^{-8}$, similar to the ones observed for 1E 2259+586, was also reported by the same authors. Up to date, the last glitch seen from 4U 0142+61 occurred on July 2011, it had a fractional frequency change of 4.44 $\times 10^{-6}$ Hz and was radiatively quiet (i.e. no burst or flare accompaining the event).

The spectral features of 4U 0142+61 had developments parallel with its timing activities. That is, in the 2000-2006 interval, the *XMM-Newton* spectra of the source, in the soft X-ray energy band (0.5-10 keV), had a quiescent phase with relatively stable total flux and spectral index over time, and it is described by a black-body plus a power-law model with the values of kT$\simeq$ 0.41 keV and photon index $\Gamma \sim 3.88$ respectively [75]. The spectra in the hard X-ray band is studied in details by den Hartog et al. [21] using the observations of four satellites *RXTE*, *INTEGRAL*. They detected emission up to 150 keV, and using phase resolved spectrocopy, showed that the source posses at least three pulse components with different spectra for 4U 0142+61. (see also [58]).

Hints of possible fall back disk around 4U 0142+61 are suggested by Chakrabarty et al. [14] based on the fact that the source is detected to be brighter in mid-infrared than in near-infrared regime. They also suggested that all the AXPs can be bright in mid-infrared regime because of surrounding fossil disks.

2.2.2 1E 2259+586

AXP 1E 2259+586 is a magnetar found in the supernova remnant SNR G109.1-01.0. It was discovered by Fahlman and Gregory [33] and it is the first AXP known. For the first years after the discovery, AXP 1E 2259+586 was classified as a binary system ([7]; [66]); however, Kaspi et al. [52] showed that the source was stable for more than 2.6 years so they classified it as a magnetar instead.

According to the most recent timing studies of the source, 1E 2259+586 is known to have a pulse period around 7 s and a period derivative of 0.05×10^{-11} s/s [23]. The inferred dipole magnetic field strength and characteristic age are 0.59×10^{14} G and 230 kyrs, respectively. The distance of the source is found to be 4.0 ± 0.8 kpc [85]. 1E 2259+586 has a luminosity of $L_x = 1.8 \times 10^{34}$ erg/s ([41]; [44]; [69]).

1E 2259+586 entered an active burst phase on June 2002 when more than 80 short SGR-like bursts were reported [38]. The flux level increased by a factor of more than 20 and a glitch with an amplitude of $\frac{\Delta\nu}{\nu} \sim 4.24 \times 10^{-6}$ accompanied with this outburst ([54]; [92]). Woods et al. [92] modeled the spectra with a black-body plus a power-law fit before and after the burst active phase using the *RXTE* and *XMM-Newton* observations and they found that several parameters like black-body temperature, photon index,and pulsed fraction changed during the burst. However, the recovery time span of these parameters were within few days. After the burst phase, the source entered a quiescence phase that lasted for more than 4 years before it had the second fractional frequency change with a value of $\sim 8.5 \times 10^{-7}$([25]; [22]; [45]). The same authors showed that the second glitch was radiatively quiet and had no recovery phase. İçdem et al. [45] also showed two micro-glitches (small fractional changes) of values $\frac{\Delta\nu}{\nu} = 3.08(32) \times 10^{-8}$ and $\frac{\Delta\nu}{\nu} = -1.39(11) \times 10^{-8}$, interpreted as positive and negative micro-glitches and resembled them with the ones seen in radio pulsars. The last time 1E 2259+586 experienced a glitching event was on April 2012 [3]. The net spin-down frequency of the source decreased 2-3 times and had a negative value of $\Delta\nu \sim -2 \times 10^{-7}$ Hz, that is why they call it an anti-glitch [3].

The spectral analysis of 1E 2259+586 show that the spectra of the source in the

0.6-12.0 keV band can be modeled by a black-body and a power-law of kT = 0.400(7) keV and $\Gamma = 3.75$ respectively [95]. The modeling components of the high X-ray energy band (> 20keV) are not known yet. In addition to X-ray emission, 1E 2259+586 has been detected in mid-infrared to far-infrared [58].

2.2.3 1RXS J170849.0–400910

AXP 1RXS J170849.0–400910 was firstly discovered in 1996 with ROSAT satellite [90]. The classification of 1RXS J170849.0–400910 as an AXP was done by Israel et al. [47]; [46] when they measured the spin-down rate to be $\sim 2\times10^{-11}$ s/s. The pulse period of the source is 11 s and the period derivative is 1.94×10^{-11} s/s [23]. The $P-\dot{P}$ combination yield a dipole magnetic field strength of $\sim 4.7\times10^{14}$ G, typical of a magnetar. The distance is estimated to be ∼3.8kpc and the luminosity in the soft X-ray band (2-10keV) $\sim 1\times10^{35}$ erg/s [29]. The characteristic age ($\tau = P/2\dot{P}$) is $\sim$ 9.0 kyr.

The timing characteristics of 1RXS J170849.0–400910 has been studied almost completely by using the data of *RXTE*. This satellite has been monitoring 1RXS J170849.0–400910 for almost 14 years, from the discovery of the source in $\sim$ 1997 until the end of the satellite mission in 2012. The data of first several months of *RXTE* observations showed that the source was rotating relatively stable ([47];[52]); however, this idea soon became irrelevant when the first glitch occurred [55]. The event occurred on October 08, 1999, the fractional frequency change was $\frac{\Delta\nu}{\nu} \simeq (6.2 \pm 0.3) \times 10^{-7}$, it had a slow, almost linear recovery and it was recorded as the first glitch ever reported from an AXP. Almost 1.5 years later, on April 15, 2001 the second glitch was observed ([53]; [18]. It had a magnitude of $\frac{\Delta\nu}{\nu} \simeq 1.4 \times 10^{-7}$ and unlike the first one, the second glitch had an exponential recovery with a time scale of $\sim$ 50 days. The third glitch was near June 30, 2005, it had a relatively large fractional frequency change of $\frac{\Delta\nu}{\nu} \sim 2.7 \times 10^{-6}$ and, like the first glitch of this source, it had no obvious recovery [25].

The last glitch known so far is reported by Scholz et al. [77] using *SWIFT* observations. The exact date of the event is not known but it is reported to

be within 11 days interval around MJD 56019 (April 2, 2012). The fractional frequency change was $\frac{\Delta\nu}{\nu} = (8.3 \pm 0.6) \times 10^{-7}$ and it had an exponential recovery similar to the second glitch of this source reported by Dib and Kaspi [25] only that the recovery timescale was 111 ± 15 days, more than 2 times larger than the second glitch. In addition to the certain glitches, two glitch candidates and three timing anomalies are reported in the literature for 1RXS J170849.0–400910 [23].

A very prominent characteristic of 1RXS J170849.0–400910 is that it shows a correlation between the X-ray flux and spectral hardness [74]. Using the *XMM-Newton* data they showed that the more the X-ray flux increases, the harder the X-ray spectra become, where peaks of both quantities are near the epochs of 1999 and 2001 glitches. This correlation was further confirmed by using data from *CHANDRA* and *SWIFT* satellites in the soft X-ray band [13], and from *INTEGRAL* in the hard X-ray band [40]. The widely accepted explanation standing behind this phenomena is the one published in the paper of Beloborodov and Thompson [8] where they state that, the star's magnetosphere may have periodic twisting/untwisting behavior.

2.2.4 1E 1841–045

1E 1841–045 was firstly identified in 1985 as a pulsar located at the center of the Supernova Remnant Kes73 [57]. The first spin period of this source was measured using the data of *ASCA* and it was found to be ~ 11.8 s, and it was classified as an AXP [89]. The latest studies show that 1E 1841–045 has a spin-down rate of 4.09×10^{-11} s/s [23]. The dipole magnetic field strength implied from P and $\dot{P}$ values is calculated to be $\sim 7.1 \times 10^{14}$ G. 1E 1841–045 is located in the galactic plane at a distance of ~ 8.5 kpc [84] and because of the large interstellar absorption, the infrared or optical counterparts are not identified yet (if there are any).

The timing of 1E 1841–045 was studied for the first time by Gotthelf [39] using the archival data of *Ginga*, *ASCA*, *ROSAT*, *RXTE* and *BeppoSAX* satellites from 1993-1999. The results of this study showed that the spin-down rate of this source was constant, that the pulse profile was unvarying and that the flux

was persistent. The next long-term timing solution of 1E 1841–045 was presented by Dib et al. [25] using the data taken with *RXTE* satellite from 1999-2008. They reported three glitches from this source; the first one occurred in July 9, 2002 and had a value of $\frac{\Delta\nu}{\nu} = 5.63 \times 10^{-6}$, the second one was on December 24, 2003 and had a value of $\frac{\Delta\nu}{\nu} = 2.45 \times 10^{-6}$, and the third one occurred on March 29, 2006 and had a value of $\frac{\Delta\nu}{\nu} = 1.39 \times 10^{-7}$ [25]. The fourth glitch of 1E 01841–045 had a value of $\frac{\Delta\nu}{\nu} = 5.5 \times 10^{-6}$. Dib and Kaspi[23] showed that the long term time variability is composed of only these glitches.

Being in a quiescence mode since its discovery, 1E 1841–045 entered an active phase in between May 2010- July 2011 where nine bursts occurred [62]. The total energy released from all nine burst is of the order of $\sim 8 \times 10^{39}$ ergs, where the energy of each burst was varying from $0.8 - 25 \times 10^{38}$ ergs and the time duration of them ranged between 18-140ms [62]. The spectral and temporal properties of 1E 1841–045 resemble very much the ones of (SGR) bursts but the energy range is on the low side of SGR bursts ([62]; [94]). When SGRs are in their active phase, they emit thousands of short bursts, whereas 1E 1841–045 emitted only nine in total. Moreover, the persistent X-ray emission remained almost unchanged even after the active phase, unlike most AXPs [62].

Using the *XMM-Newton data*, the spectra of 1E 1841–045 in the soft X-ray band (0.5-10 keV) is modeled by a black-body plus a power law with kT $= 0.45 \pm 0.03$ keV and $\Gamma = 1.9 \pm 0.2$, respectively [60]. Hard X-ray spectra of this source was investigated by Molkov et al. [68]; Kuiper et al. [59]; Kuiper et al. [58]. Using *RXTE* and *INTEGRAL* data, they measured a powerlaw index of $\Gamma \sim 1.3$ and showed that the pulsed fraction in 20-300 keV is high. No information is yet available for emission of this source in other wavelengths.

CHAPTER 3

SATELLITE AND OBSERVATIONS

This chapter is dedicated for the X-ray satellite of which all the relevant data are gathered from, namely *Rossi X-ray Timing Explorer (RXTE)*. The properties of the satellite as well as its working principles will be discussed. All the related information in this section about *RXTE* spacecraft is gathered from *RXTE* Guest Observation Facility (GOF) webpage[1]. In additon, list of observations and the data used are illustrated.

3.1 The Rossi X-ray Timing Explorer

RXTE was a satellite designed mainly to study the X-ray timing and spectral properties of the sources in the 2-200keV energy band ([50]; [80]; [11]). It was lunched on December 30, 1995 from NASA's Kennedy center by Delta rocket II, and after 16 years it was decommissioned on January 5,2012. The altitude and orbital inclination of this satellite was $\sim$ 600km and 23 degree respectively. *RXTE* had a maneuvering capacity of 6 degree per minute and it could point almost at any position on the sky. The only exception was when it was positioned closer than 30^{o} towards the Sun, when it was orbiting near South Atlantic Anomaly (a region with particle flux anomaly) and when there were Earth occultations.

The board of *RXTE* spacecraft had three instruments: Proportional Count Array (PCA), High Energy X-ray Timing Experiment (HEXTE), and All Sky Mon-

[1] http://heasarc.gsfc.nasa.gov/docs/xte/xte_1st.html

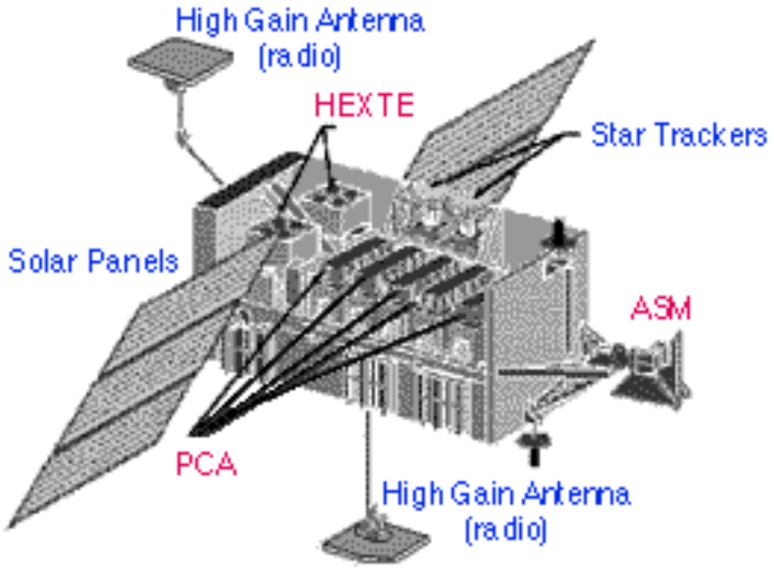

Figure 3.1: The instruments of *RXTE* satellite.[2]Among these instruments PCA detector is used in this study.

itor (ASM). The Figure 3.1 shows the location of the instruments on spacecraft of *RXTE*. PCA and HEXTE were designed to measure the timing variability up to microsecond level. The ASM used to be responsible for the brightest sources of the sky and identified the newly X-events happening on the sky. For this reason ASM was programmed to scan more than 80% of the sky every 1.5 hour. In this thesis, only the data taken by PCA detector is used for carrying out our analysis.

3.1.1 Proportional Counter Array

Proportional Counter Array (PCA) was composed of five identical Proportional Counter Units (PCUs) as showed in the Figure 3.1. This instrument had a total area $\sim 6500cm^2$, was effective in 2-60 keV energy range, had 256 spectral channels and was collimated to 1 x 1 degree field of view (FOV) [50].

Briefly, the instrument detection occurs with scheme: When a photon came, it firstly entered the collimator. The aim of the collimator was to limit the field of view of sky, the off-axis photons were absorbed by the collimator. Once the

[2]retrieved from webpage http://heasarc.gsfc.nasa.gov/docs/xte/XTE.html

collimator path was finished, the photons pass through the first mylar window and reach the propane layer. The aim of the mylar windows was to let the X-rays pass through while preventing the propane gas from escaping. The propane gas was located in between the mylar windows and it served as an anti-coincidence layer, a layer that acts as a detector for the charged particles. When those charged particles entered through the propane layer they use to excite the gas, and this excitement was registered as a signal. Signals that were registered from both, the propane layer and one of the 5 detectors were classified as background events.

The next place the photons enter (after passing the second mylar window too) was the main detector. This part of the PCU was filled 90% with xenon and 10% with methane gas. The xenon gas gets highly ionized by the photons of 2-60 keV, it is inert and not electronegative, these properties prevent the gas from reacting react with the other parts of the detector. Meanwhile methane served as a 'tool' to catch the UV photons when incorrectly created from the excitement of the xenon gas. Once a photon interacts with the xenon gas it forms an electron-ion pair. Because of the potential difference created, electron goes toward anode and ion goes toward cathode. In its way to anode this electron collides with other gas molecules and create another electron, and so on until an avalanche of electrons were created along their way to anode. When it reached the anode this avalanche was registered as a signal. The key to understand this process was to know that the energy of the incident photon was proportional to the number of the electrons reaching the anode. It was this proportionality from where Proportional Counter Array took the name. Ions were formed as well, but they were much heaver so they use to move very slowly and rarely interacted. Another anode was in the bottom of the detectors. The aim of this anode was to detect the charged particles coming from outside in the bottom part. All the events that were registered in this anode and in any other anode of the detector were classified as background events and were discarded.

3.1.2 Experimental Data System

The data collected on PCA did not transferred to Earth directly because of their big data size. Instead, this data was firstly selected (according to the observers requests) and compressed on board by an electronics called Experimental Data System (EDS). EDS was composed of eight Event Analyzer (EA), six of which work for the PCA and only two work for ASM. EAs could record the PCA data in seven basic modes according to the observers needs. Those modes were: Event Data Mode, Binned DataMode, Burst Catcher Mode, Pulsar Fold Mode, Fast Fourier Transform Mode, Delta Binned Mode and Single Bit Mode. In this thesis only the Event Data Mode is used to analyze the data. This mode tags each photon with its arrival time and energy, and registers them as events. Moreover, all 256 energy channels of PCU were available in this mode. Event Data Mode had three configuration modes:

1. Good Xenon mode deal with all the photons in the xenon layer after the background subtraction;

2. Good xenon with propane mode operate the same as Good Xenon configuration with the addition of the events which occur in the propane layer;

3. Transparent mode work for all the signals, including those coming from background events.

Only the first two configuration modes are used in this thesis.

After the processing of EAs was done, data was packetized and transferred to the memory of the spacecraft and was ready be transmitted into the ground.

3.2 Observations

The selected AXPs are almost continuously monitored with the *RXTE* satellite during its life span for 16 years. These observations produce a great opportunity for detailed investigation of the timing parameters of these sources. With this monitoring program, the timing characteristics of 4U 0142+61, 1E 1841–045, 1E 2259+586 and 1RXS J170849.0–400910 were extensive studied by [23]. Dib and Kaspi [23] divided the time intervals for frequency measurements depending on existence of timing anomalies or glitches. In this thesis, same observations are used with an additional aim of calculating the noise strengths. The data is obtained from HEASARC data archive webpage.

Table3.1: *RXTE* observations of 4U 0142+61

Proposal Number (pnrb)	Start Date (MJD)	End Date (MJD)	Number of Observations	Total Exposure (seconds)
20146	50411.7	50795.5	14	14130
50082	**51610.6**	**51950.3**	**15**	**45363**
60069	**51986.3**	**52282.2**	**9**	**46435**
70094	**52339.6**	**52634.4**	**9**	**94945**
80098	**52726.2**	**53046.2**	**18**	**83235**
80099	**52890.4**	**52885.4**	**3**	**30276**
90076	**53066.6**	**53420.5**	**27**	**87970**
91070	**53438.1**	**53787.3**	**35**	**122659**
92005	**53837.2**	**54150.1**	**28**	**180068**
92006	**53800.1**	**54278.2**	**40**	**133857**
93019	**54290.9**	**54825.3**	**50**	**195633**
94019	**54838.7**	**55189.0**	**30**	**121511**
95019	**55203.5**	**55552.5**	**28**	**128684**
96017	55772.1	55772.9	2	9230
96019*	**55567.3**	**55917.3**	**27**	**124104**
total			335	1418100

Notes: Observation sets written in bold are used in this thesis. Superscript * indicates that observation set is partially used.

The *RXTE* observations of 4U 0142+61 started from MJD 50411 and ended at MJD 55917. During that interval, total sum of 335 observations carried out with a typical exposure of $\sim$ 4ks. The list of observations gathered with *RXTE* can

be found in table 3.1. Among those observations, we used 2 intervals. First one starts from MJD 51610 and ends at 53800 in which 117 pointing observations were taken. The second interval is in 54326 to 55762 MJD range with 122 observations. For this source almost 10 years of data used in total.

Table3.2: *RXTE* observations of 1E 2259+586

Proposal Number (pnrb)	Start Date (MJD)	End Date (MJD)	Number of Observations	Total Exposure (seconds)
10192	**50355.6**	**50356.2**	**2**	**86816**
20145	**50504.7**	**50532.8**	**10**	**123676**
20146	**50411.7**	**50795.5**	**14**	**13489**
30126	**51038.0**	**51149.7**	**12**	**141949**
40082	**51569.4**	**51630.0**	**20**	**118405**
40083	**51195.5**	**51969.9**	**19**	**60445**
50082	**51613.8**	**51970.0**	**11**	**62046**
60069	**52016.0**	**52312.2**	**10**	**57144**
70094*	**52355.2**	**52686.0**	**32**	**182079**
80098	**52713.6**	**53053.1**	**31**	**127331**
90076	**53067.6**	**53418.6**	**34**	**126642**
91070	**53437.3**	**54165.0**	**76**	**157633**
92005*	**54204.2**	**54205.9**	**2**	**12195**
92006	53801.0	54278.3	85	128684
93019	54284.1	54825.3	95	376733
94019*	**54832.2**	**55195.1**	**49**	**229905**
95019	**55203.3**	**55560.3**	**58**	**254653**
96019	**55567.2**	**55924.2**	**56**	**248447**
total			614	2508272

Notes: Observation sets written in bold are used in this thesis. Superscript * indicates that observation set is partially used.

Observations of 1E 2259+586 covers 5422 days in between MJD 50504 and 55924. The observations are held relatively high in number due to the timing active phase of the source after 2002. The *RXTE* gathered total sum of 614 observations with ~ 4 ks in average. The journal of observations listed in table 3.2. For 1E 2259+586, 3 different time segments are used. For the first segment, there are 103 observations starting from MJD 50356 till 52398. The second segment has 226 observations covering a range from MJD 52503 to 54180. The third and last segment for this source start from MJD 54852 and ends at MJD

Table3.3: *RXTE* observations of 1RXS J170849.0–400910

Proposal Number (pnrb)	Start Date (MJD)	End Date (MJD)	Number of Observations	Total Exposure (seconds)
30125	50825.8	51186.7	29	72783
40083	51215.8	51614.2	20	59698
50082*	**51655.7**	**52041.6**	**13**	**11648**
60069	**52035.6**	**52325.7**	**8**	**24820**
60412	**52049.5**	**52052.3**	**5**	**10027**
70094	**52366.6**	**52718.7**	**12**	**60543**
80098*	**52745.8**	**53058.7**	**58**	**113954**
90076	53063.1	53429.1	70	138381
91070*	**53435.1**	**54210.8**	**55**	**103567**
92006	**53799.0**	**54275.6**	**55**	**106409**
93019*	**54282.3**	**54785.8**	**67**	**130609**
94019	54836.8	55151.0	43	85151
95019	55202.8	55516.9	45	88507
96019	55568.0	55882.2	45	248447
total			525	1254544

Notes: Observation sets written in bold are used in this thesis. Superscript * indicates that observation set is partially used.

55924 with a total observation number of 160. Total time span of 13 years is covered.

1RXS J170849.0–400910 was also monitored for almost whole *RXTE* life span ($\sim$ 16 years), during which 525 pointing observations were held. These observations had an average exposure time $\sim$ 2400 seconds which yielded a total exposure of $\sim$ 1.25Ms (see table 3.3 for details). Among those 525 pointing observations, 2 time segments are used with 74 and 124 observations, respectively. The first of these segments in MJD 52035 to 52960 range, while the second is in MJD 53555 to 54540 range.

Continuous monitoring program for AXPs, also include AXP 1E 1841–045. The observations of this source ranges from MJD 51224 to MJD 55587. During that time interval, 277 observations are carried out with a average exposure of $\sim$ 4600 sec (table 3.4).The data used in this thesis covers time span ranging in between MJD 51224-52437,53030-53815 and 54307-55538 respectively (number of observations 56, 76 and 91 respectively).

Table3.4: *RXTE* observations of 1E 1841-045

Proposal Number (pnrb)	Start Date (MJD)	End Date (MJD)	Number of Observations	Total Exposure (seconds)
40083	**51224.5**	**51597.3**	**27**	**122209**
50082	**51644.5**	**51976.9**	**16**	**62778**
60069	**52001.6**	**52300.2**	**8**	**54906**
70094*	**52349.8**	**52666.0**	**7**	**63136**
80098*	**52726.9**	**53052.9**	**18**	**73326**
90076	**53073.8**	**53413.3**	**21**	**73856**
91070	**53440.0**	**54195.9**	**34**	**124958**
92006*	**53800.9**	**54279.6**	**31**	**144676**
93017*	**54328.6**	**54330.2**	**3**	**14631**
93019	**54293.5**	**54807.2**	**37**	**172557**
94019	**54860.1**	**55168.2**	**22**	**97448**
95017	**55323.6**	**55329.3**	**6**	**41853**
95019	**55223.0**	**55538.0**	**24**	**111868**
96019	55587.8	55903.3	23	115399
total			277	1273331

Notes: Observation sets written in bold are used in this thesis. Superscript * indicates that observation set is partially used.

CHAPTER 4

TIMING ANALYSIS

As mentioned in previous chapters, In order to investigate the properties of magnetars, measuring exact rotation period and its spin-down rate is crucial. Remarkable physical information, such as estimation of dipolar magnetic field strength and glitches in the rotation period and much more, can be gathered from spin period and spin down rate measurements. In this thesis, phase coherent timing technique is applied for measuring the pulse arrivals of these objects. Then rotational parameters, such as spin periods and its higher derivatives, are obtained.

4.1 Data reduction

Prior to initiate an analysis, obtained data must be prepared carefully in order to make sure that calculated results are accurate. In this thesis, data taken by *RXTE* satellite is used, so briefly explanation below aims to clarify the data reduction steps. In chapter 3, the rough scheme that how *RXTE* satellite conducts its observations is given. More information about data reduction tools for *RXTE* satellite can be found on HEASARC *RXTE* GOF webpage[1].

Once an observation is made, all the events happened during these observations are gathered. And all of them are recorded as "flexible image Transport System", known as FITS format in short. Within this file format, arrival times and energies of photons are recorded as well as information about in which PCU

[1] http://heasarc.gsfc.nasa.gov/docs/xte/data_analysis.html

layer its detected. In addition, for example, in the header of the event file, information regarding start date, end date, exposure time, pointing direction, time resolution and much more can be found. The position of the satellite in sky is registered in orbit files. And many technical information such as South Atlantic Anomaly Passage, offset of pointing from the selected object, electron rate of each PCU, and high detector voltages are recorded in filter files.

For our analysis, we filtered out these data for Earth occultations by setting elevation angle to be less than 10 degrees. Additionally, in order to retrieve the photons which are captured during stable pointing observation, pointing offsets less than 0.02 degrees are selected. Moreover, time since South Atlantic Anomaly is kept to be both less than 0 and higher than 30 minutes for avoiding the high energy particle flux that would lower our signal to noise ratio during these SAA passages. Using science event extract (`seextrct`) tool, the time series (lightcurves) are obtained from these filtered events for the 3-20 keV energy band. And the these lightcurves are binned with 0.05 seconds. The resulting time series in the lightcurves are adjusted to the solar system barycenter reference frame so that arrival times of photons are not delayed by the orbital motion of the satellite and observations can be assumed to be taken place in an inertial frame. Additionally, we corrected these lightcurves of PCU on/off status by the tool `correctlc`. The final lightcurves are held subject to timing analysis.

4.2 Power Spectrum

General method for searching a periodic signal in a lightcurve is the power spectrum extraction [87]. In this method, the lightcurve which is in time domain is converted into frequency domain via Fourier Transformation (FT). In other words, if the data is represented by $C_n(t)$, then the Fourier transformation of it is represented by;

$$H_k = \frac{1}{N} \sum_{k=0}^{N-1} C_n e^{2k\pi\nu T/N} \tag{4.1}$$

where C_n is counts of time bin n, N is the total number of bins of the data, T is the time span of the data and ν is the frequency. Then the power of the signal

P_k can be estimated as;

$$P_k = H_k(\nu)H_k^*(\nu) =\mid H_k \mid^2 \tag{4.2}$$

where $H_k^*(\nu)$ is the complex conjugate and $\mid H_k \mid$ is the absolute value of $H_k(\nu)$. If the time resolution of the data is Δt, then the frequency resolution is $\Delta\nu = \frac{1}{N\Delta t}$. The transformation is carried out for all frequencies up to a maximum frequency which is defined as;

$$\nu_{max} = \frac{1}{2\Delta t}. \tag{4.3}$$

The maximum frequency ν_{max} is also referred as Nyquist frequency. With this transformation, only the periodic signals are amplified. When the power spectrum (i.e the frequency versus power amplitude plot) is generated, a periodic signal (e.g. pulse period) of a source can be clearly identified with the frequency resolution $\Delta\nu$. In this study, the power spectra are generated by the tool `powspec` of ftools software.

4.3 Phase Coherent Timing

Magnetars are pulsating objects which means that they exhibit periodic modulations in their lightcurves. As discussed in previous chapters, these modulations are associated with their spin period. Phase coherent timing technique is a widely used method for investigating the time variations of such periodic modulations.

Although magnetars spin down rapidly (in the orders of 10^{-11} s/s), their spin periods can be assumed to be roughly constant over one single observation which typically has a few thousand seconds of duration. Under that assumption, starting from an epoch the time series are folded over the given periodicity in order to obtain more stable and high signal-to-noise ratio pulse profiles. Created pulse profiles will have number of bins N, depending on the choice. In this thesis, we choose 20 bins for the pulse profiles which provides enough accuracy for pulse arrival measurements. Each observation is held subject to "epoch folding". Therefore, one pulse profile is obtained for each observation. The spin

frequency of the object as a function of time can be written as:

$$\nu(t) = \nu_0 + \dot{\nu_0}(t - t_0) + \frac{1}{2}\ddot{\nu_0}(t - t_0)^2 + \frac{1}{6}\dddot{\nu_0}(t - t_0)^3 + ... \tag{4.4}$$

where t_0 is the starting time of epoch folding, ν_0 represents the initial spin frequency at time t_0 and $\dot{\nu}$ is its first derivative $\frac{d\nu}{dt}$ and so on. But since epoch folding gives pulse profiles, the information we have is on phase domain. So, the above equation needs to be converted to phase. The relation between phase and frequency is;

$$\Phi(t) = \int \nu(t)dt \tag{4.5}$$

where $\phi(t)$ is phase as a function of time. By integration the equation 4.1, we can obtain the $\Phi(t)$ as follows:

$$\Phi(t) = \Phi_0 + \nu_0(t - t_0) + \frac{1}{2}\dot{\nu_0}(t - t_0)^2 + \frac{1}{6}\ddot{\nu_0}(t - t_0)^3 + ... \tag{4.6}$$

where Φ_0 is the initial phase at time t_0 and originated from integration constant.

In order to construct the $\Phi(t)$, one of the pulse profiles should be used as a reference which is known as "master" or "template" pulse profile. The master pulse will be chosen by the most statistically strong (maximum χ^2) profile. If there were no signal (i.e; no pulse), the counts in the bins of the pulse profile will be approximately equally distributed. Denoting counts in the bin i as c_i and average count rate of the profile as $\langle c \rangle$, The χ^2 of a profile can be calculated as;

$$\chi^2 = \frac{1}{N-1}\sum_{i=0}^{N-1}(\frac{c_i - \langle c \rangle}{\sigma_i})^2 \tag{4.7}$$

where σ_i is the standard error of count rate c_i. If the signal is weak,i.e; $c_i \simeq \langle c \rangle$, the χ^2 will be low. And if the signal is strong, it will produce high χ^2. So, among the pulse profiles, the master pulse will be chosen according to its χ^2. Then, the resultant master pulse can be represented as harmonics via [20]:

$$g(\Phi) = G_0 + \sum_{k=1}^{m} G_k cosk(\Phi - \Phi_k) \tag{4.8}$$

where G_0 is a constant, summation upper limit m is the number of harmonics, Φ is phase and Φ_k is the initial phase offset. The number of harmonics m of the pulse representation should be less than half of the number of the bins N/2.

And the remaining pulse profiles can be assumed to have the approximately same shape but they may differ in pulsed flux or arrival time. The deviations of each pulse from the master pulse can be obtained by cross correlation. The offset of these pulses can be obtained via [20];

$$\Delta\Phi = \frac{\sum_{k=1}^{m} kG_kF_kcosi\Delta\Phi_k}{\sum_{k=1}^{m} k^2G_kF_kcosk\Delta\Phi_k} \tag{4.9}$$

After the cross correlation, phase shift of each pulse from the master pulse is calculated. It brings a condition that number of rotations between one observation to another is an integer (plus the phase shift we obtained). However, the cost it brings will be the chance of miscounting the rotational cycles if there is a large time gap in between two consecutive observations. But still, it has to be an integer multiplicative of rotation cycles. Once the all the pulse arrivals are evaluated by this method, the equation 4.3 can be used as a model for the arrival times. Hence, rotational parameters of the object will be extracted. And it is most commonly referred as timing solution. Of course the model (equation 4.3) has to be modified in case of an orbital modulation (e.g. for binaries) or an any timing anomaly.

4.4 Timing Noise

Even though, pulsars and magnetars seem to be rotating in a very regular fashion, there are still small random fluctuations in their spin frequencies. These random fluctuations are still present even after the subtraction of high order polynomials (i.e: spin-down rate or higher derivatives). The random fluctuations in the residuals of pulse timing is referred as timing noise. Boynton et al. [10] considered three cases for the timing noise:

1) *random walk in phase* which indicates emission region is changing or beam direction is shifted. In that case, root mean square (r.m.s) of residuals should scale with time as $T^{1/2}$.

2) *random walk in frequency* which may originate from alterations of moment of inertia of the object. In that case, r.m.s would scale in time as $T^{3/2}$.

3) *random walk in spin-down rate* which is related with the energy loss pro-

cesses. The r.m.s values of residuals of timing solution would propagate as $T^{5/2}$ in time.

Then the variance $< \Delta\Phi >_r$ (i.e. square of r.m.s.) should scale in time as $S_r T^{2r-1}$ where r is an integer which indicates the order of the red noise. The coefficient S_r would depend on the order of polynomial used for extraction, and can be calculated using the actual mean square residuals of the data and its expected value [19].

$$< \sigma_r^2 >_a = S_r T^{2r-1} < \sigma_r^2 >_e \tag{4.10}$$

where subscript a and e refers to "actual" and "expected", respectively. The expected value can be either calculated mathematically [19] or by Monte Carlo Simulations [17]. Using the expected values and r.m.s of residuals, noise strength amplitude S_r can be obtained.

CHAPTER 5

RESULTS

In this chapter, analysis results of selected AXPs (4U 0142+61,1E 2259+586, 1RXS J170849.0–400910 and 1E 1841–045) will be presented. Conducted data reduction and analysis methods towards our aim in this section are presented in Chapter 4. In this thesis, timing solution of this object is reanalyzed for glitch free regions so that residuals are not affected by glitches. Because the contributions of glitches to residuals would mislead the noise strength estimation.

5.1 4U 0142+61

As mentioned in chapter 3, AXP 4U 0142+61 had been monitored with *RXTE* for about 16 years. A detailed timing analysis of this source is done by Dib et al. [24].

Table5.1: Timing Ephemerises of AXP 4U 0142+61

	Start Date (MJD)	End Date (MJD)	Time Span (Days)
Ephemeris A	50170	50893	723
Ephemeris B	**51610**	**53800**	**2190**
Ephemeris C*	**53831**	**54867**	**1036**
Ephemeris D*	**54881**	**55762**	**881**
Ephemeris E	55777	55917	140

Notes: Ephemerises given in this table are defined in [23]. Ephemerises written in bold are used in this thesis. Ephemerises with **(*)** are combined into one single interval

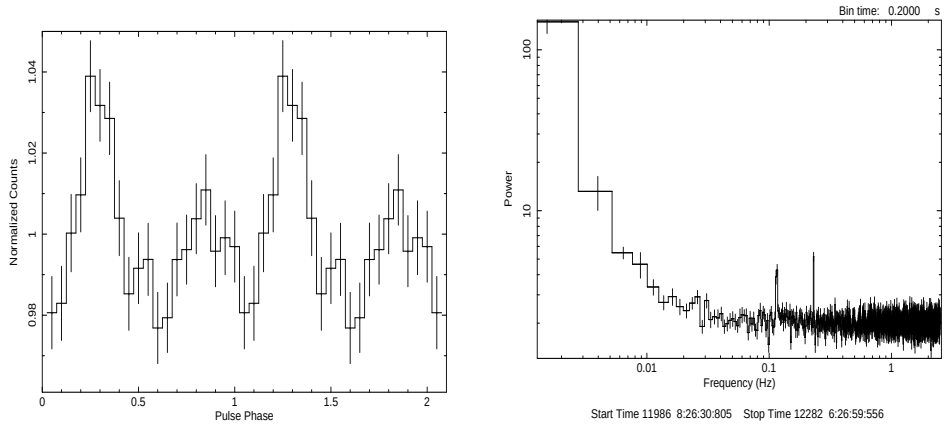

(a) (b)

Figure 5.1: **(a)** Sample pulse profile of AXP 4U 0142+61, **(b)** Power Spectrum of AXP 4U 0142+61 obtained from *RXTE* observations (observation set P60069). The source signal at ~ 0.115 Hz and its second harmoni at ~ 0.230 Hz can be noticed.

and timing parameters are calculated from observations between MJD 50170 - 53787 (ephemeris A & B in the table 5.1). Their solution make use of high order derivatives (up to 6th) due to the fact that there exist a two years of gap in the data. When timing parameters before and after the gap investigated more closely, they concluded that cubic or quadratic fits can reflect the data well. Later in 2014, Dib et al. [23] expanded the timing solution to MJD 55917.They performed the analysis in five segments pivoting on timing events (see table 5.1). Time averaged spin-down rate yielded -2.68×10^{-14} Hz/s.

Table5.2: Timing parameters of AXP 4U 0142+61

	Epoch (MJD)	Frequency (Hz)	Spin-down rate (10^{-14} Hz/s)
Ephemeris B	**51704.0**	**0.115096792(1)**	**-2.6546(4)**
Ephemeris B^a	53800.0	0.1150921156(7)	-2.679(5)
Ephemeris C&D	**54713.5**	**0.1150899954(3)**	**-2.6472(12)**
Ephemeris C^a	53800.0	0.1150921068(7)	-2.714(4)
Ephemeris D^a	53800.0	0.1150920514(11)	-2.621(8)

Notes: Superscript **(a)** denotes the timing parameters up to quadratic term obtained by Dib et al. [23]. The ephemerises written in bold represents the results of this study.

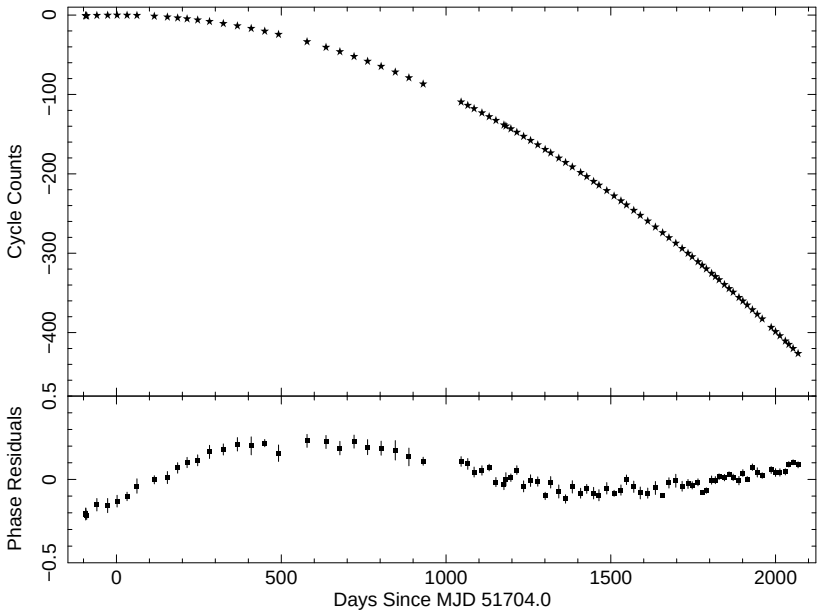

Figure 5.2: Pulse arrivals and their residuals after removal of spin-down trend of 4U 0142+61 for the ephemeris B.

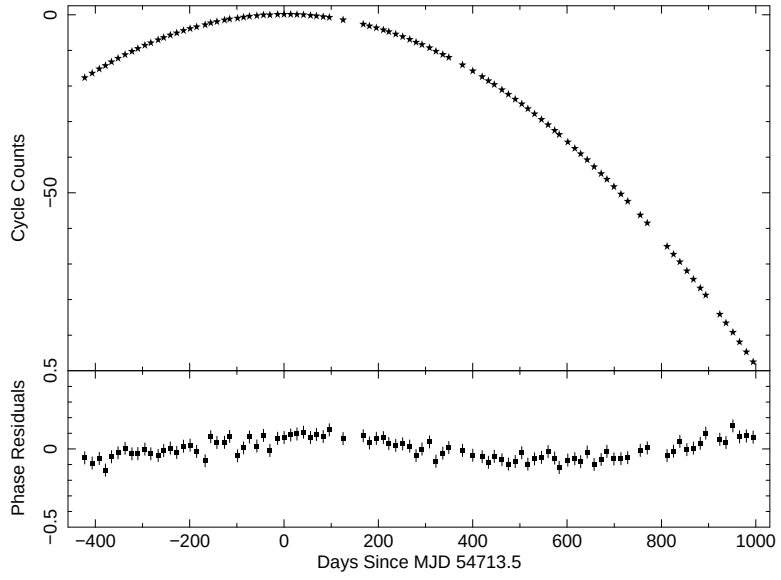

Figure 5.3: Pulse arrivals and their residuals after removal of spin-down trend of 4U 0142+61 for the ephemeris C&D.

Among the five segments, we have used only the intervals B, C and D to estimate the timing noise of 4U 0142+61 due to their longer time span. However; C and D segments are combined in to one because the glitch candidate reported depends on one single TOA [23]. We omitted that one TOA from our analysis.

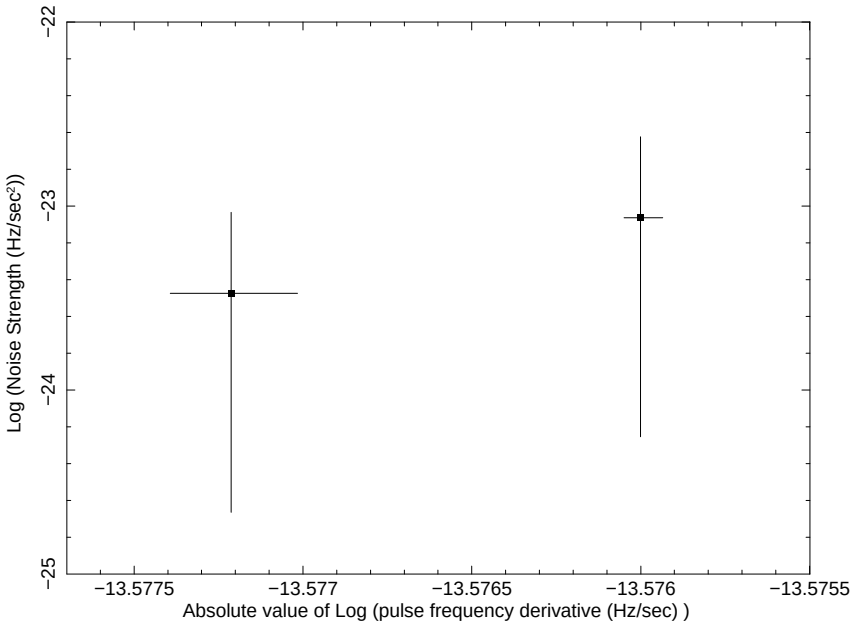

Figure 5.4: Logarithm of timing noise strength as a function of logarithm of absolute value of the spin-down rate for AXP 4U 0142+61, each point corresponds to the time intervals defined in table 5.2.

First, a sample power spectrum is constructed using the observation set 60069 to demonstrate the signal at ~ 0.115 Hz and its harmonic at ~ 0.230 Hz emerging from this source (figure 5.1b). Using the epoch and the frequency for the selected segments, pulse profiles are built from the lightcurves of 3-20 keV (see figure 5.1a for a sample pulse profile). The phase coherent timing technique is used to measure pulse arrivals. The parameters estimated from the modeling of pulse arrivals using the equation 4.3 up to quadratic polynomial are listed in table 5.2, our results slightly deviate from the solution presented by Dib et al. [23] because we limited polynomial fitting up to second order and the rest is considered to be a part of the noise. Residuals remaining from the subtraction of the quadratic polynomial from pulse arrivals are used to estimate the noise strength of 4U

0142+61. Cycle counts and the residuals remaining after the quadratic removal are showed in figure 5.2 and 5.3. Also measured noise strength versus spin-down rate values for these two time segments can are plotted in figure 5.4.

5.2 1E 2259+586

Long term timing characteristics of 1E 2259+586 is recently updated by Dib et al. [23]. The time span of their study covers 16 years. They presented timing solutions for four different epochs due to glitches in the spin frequency of the source (see table 5.3 for defined ephemerises). Among those intervals, ephemeris A, B2

Table5.3: Timing Ephemerises of 1E 2259+586

	Start Date (MJD)	End Date (MJD)	Time Span (Days)
Ephemeris A	**50356**	**52398**	**2043**
Ephemeris B1	52445	52461	16
Ephemeris B2	**52503**	**54180**	**1677**
Ephemeris C	54194	54852	658
Ephemeris D	**54852**	**55924**	**1072**

Notes: Ephemerises given in this table are defined in Dib et al. [23]. Ephemerises written in bold are used in this thesis.

and D are held subject to reanalysis. The selection of ephemerises are carried out regarding their time span. Applying phase coherent timing, timing solutions are extracted for the mentioned intervals. To illustrate the signal coming from the

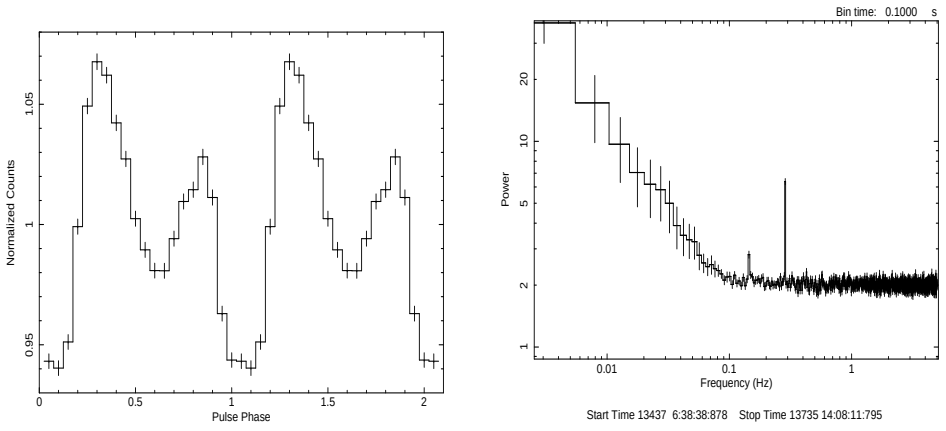

(a) (b)

Figure 5.5: **(a)** Sample pulse Profile of 1E 2259+586, **(b)** Power Spectrum of 1E 2259+586 obtained from *RXTE* observations (observation set P91070). The source signal at ~ 0.143 Hz and its second harmonic at ~ 0.286 can be noticed.

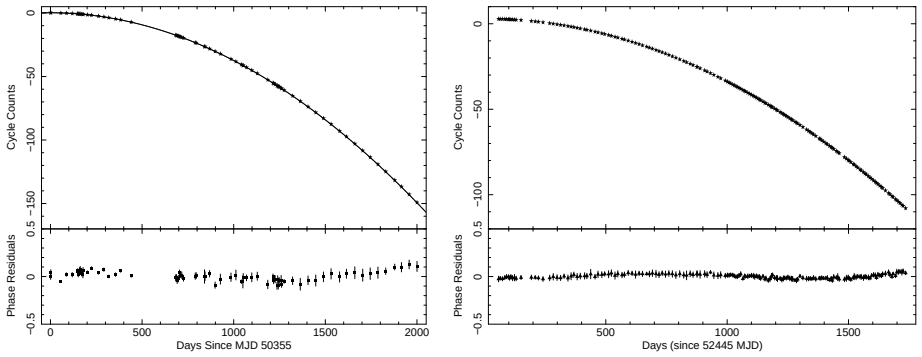

(a) (b)

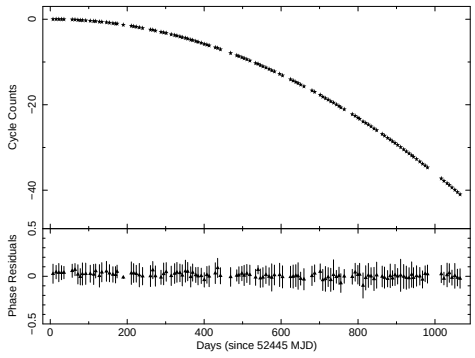

(c)

Figure 5.6: Pulse arrivals and their residuals after removal of spin down trend of AXP 1E 2259+586 for **(a)** Ephemeris A, **(b)** Ephemeris B2, **(c)** Ephemeris D

source, a sample power spectrum is created from P91070 observation set. A fact to notice is that power of first harmonic is greater than the signal at ~ 0.143 Hz indicating that pulse profile is double peaked. Lightcurves with 0.05 s binning in the 3-20 keV energy band are used. After epoch folding, pulse profiles with 20 phase bins are acquired (see figure 5.5a for a sample pulse profile). After the cross correlation of the pulse profiles with the template, phase shifts are calculated. For each interval defined above, quadratic polynomial trend is removed from the pulse arrivals. The cycle counts and their residuals after polynomial subtraction are shown in the figure 5.6. The obtained timing parameters are shown in table 5.4.

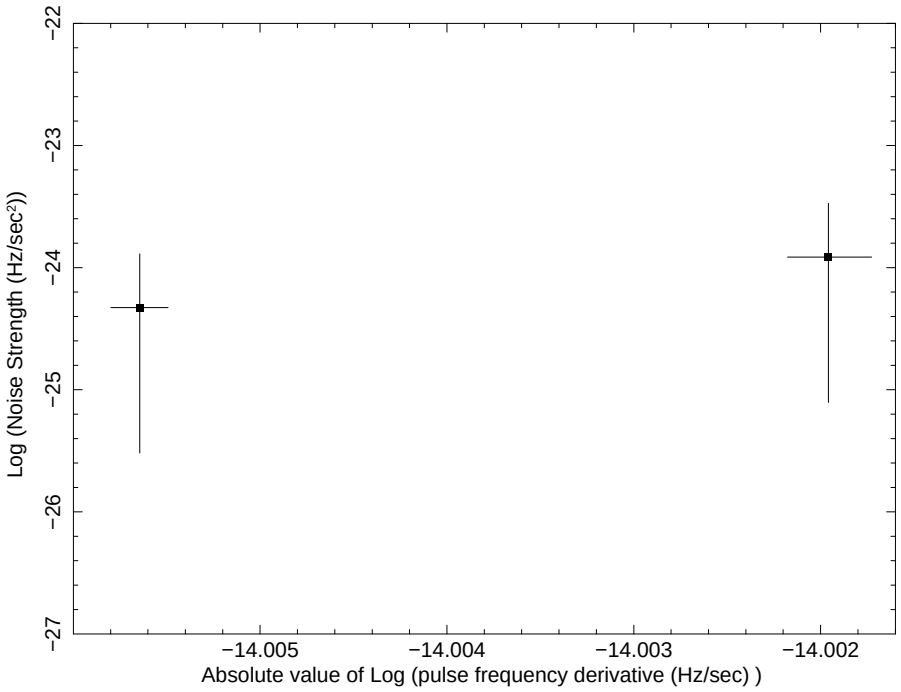

Figure 5.7: Logarithm of timing noise strength as a function of logarithm of absolute value of the spin-down rate for 1E 2259+586, each point corresponds to the time intervals defined in table 5.4.

Table5.4: Timing Parameters of AXP 1E 2259+586

	Epoch (MJD)	Pulse Frequency (Hz)	Spin down rate (10^{-15} Hz/s)
Ephemeris A	**50355.0**	**0.1432887872(3)**	**-9.955(5)**
Ephemeris A^a	50355.0	0.1432887919(2)	-10.201(17)
Ephemeris B2	**52445.0**	**0.1432874931(3)**	**-9.871(3)**
Ephemeris $B2^a$	52445.0	0.1432874928(2)	-9.729(13)
Ephemeris D	**54852.0**	**0.143285577(2)**	**-9.688(40)**
Ephemeris D^a	54852.0	0.14328554678(3)	-9.6748(7)

Notes: Superscript **(a)** denotes the timing parameters up to quadratic term obtained by Dib et al. [23]. The ephemerises written in bold represents the results of this study.

The timing parameters are slightly different from the measurements of Dib et al. [23] owing to the fact that they used higher order polynomials to represent the data.Then, for the residuals of interval A, B2 and D, the timing noise strength is evaluated. However, due to the low timing noise in Ephemeris D, only an upper limit value of the timing noise strength is obtained. Therefore, we did not use Ephemeris D for the investigation of correlation between the timing noise strength and spin-down rate (See figure 5.7). It is remarkable that the noise level sightly increases with the absolute value of increasing frequency derivative.

5.3 1RXS J170849.0–400910

As mentioned in previous section, 1RXS J170849.0–400910 is shown to be rotating with an unstable fashion, i.e; it experienced many timing discontinuities ([55]; [48]; [25]; [23]; [12]; [18]). Therefore, the most recent updated timing solution is splited into seven ephemerises to account for the discontinuities mentioned by Dib et al. [23] (see table 5.5).

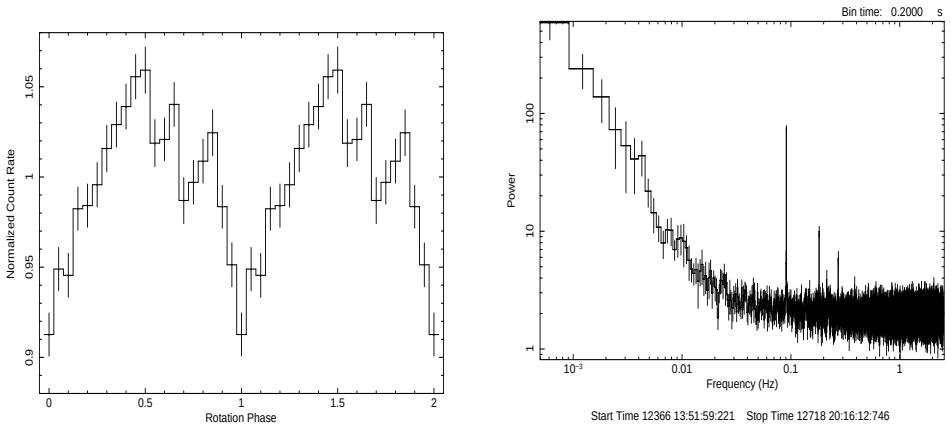

(a) (b)

Figure 5.8: **(a)** Sample pulse profile of 1RXS J170849.0–400910, **(b)** Power Spectrum of 1RXS J170849.0–400910 obtained from *RXTE* observations (observation set P70094). The source signal at ~ 0.09 Hz can be noticed.

Since the aim of our analysis is to estimate the noise strengths, we only considered the time intervals in which no timing discontinuity is observed and which has a long time span ($\sim$ 1000 days). Due to the timing discontinuities of the source, only the Ephemeris C & F are used for analysis. The time span of Ephemeris C is reduced almost 300 days for our analysis because there exists a glitch recovery in a part of the interval. 3-20 keV lightcurves with 0.05 s bins are constructed for these intervals and then subjected to pulse timing analysis. After the epoch folding, pulse profiles of 20 bins are obtained (see figure 5.8a for a sample pulse profile). Power spectrum of the source is also extracted for the first observation set. The spin frequency signal at ~ 0.09 Hz and its first and second harmonics can be seen (see figure 5.8b).

Table5.5: Timing Ephemerises of 1RXS J170849.0–400910

	Start Date (MJD)	End Date (MJD)	Time Span (Days)
Ephemeris A	50825	51418	593
Ephemeris B	51446	51995	549
Ephemeris C	**52035**	**52960**	**925**
Ephemeris D	53010	53325	315
Ephemeris E	53377	53547	170
Ephemeris F	**53555**	**54540**	**985**
Ephemeris G	54547	54785	238
Ephemeris H	54836	55516	680
Ephemeris I	55567	55882	315

Notes: Ephemerises given in this table are defined in [23]. Ephemerises written in bold are used in this thesis.

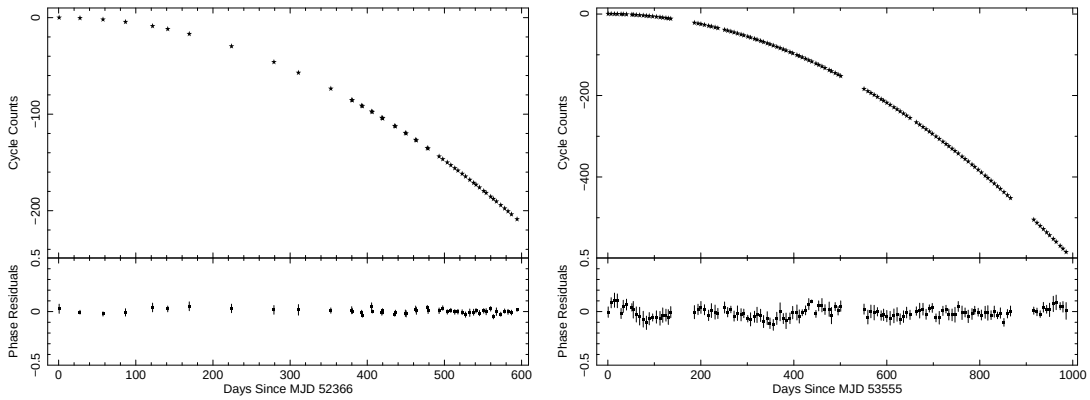

(a) (b)

Figure 5.9: Pulse arrivals and their residuals after removal of spin down trend of for 1RXS J170849.0–400910 **(a)** Ephemeris C, **(b)** Ephemeris F

Table5.6: Timing Parameters of 1RXS J170849.0–400910

	Epoch (MJD)	Pulse Frequency (Hz)	Spin down rate (10^{-13} Hz/s)
Ephemeris C*	**52366.0**	**0.090901293(2)**	**-1.5853(5)**
Ephemeris C^a	52016.48413	0.090906067(11)	-1.556(6)
Ephemeris F	**53555.0**	**0.090885183(1)**	**-1.5951(3)**
Ephemeris F^a	53555.0	0.090885255(16)	-2.38(11)

Notes: Superscript **(a)** denotes the timing parameters up to quadratic term obtained by [23]. The ephemerises written in bold represents the results of this study. Ephemeris with **(*)** covers almost 300 days less than C^a.

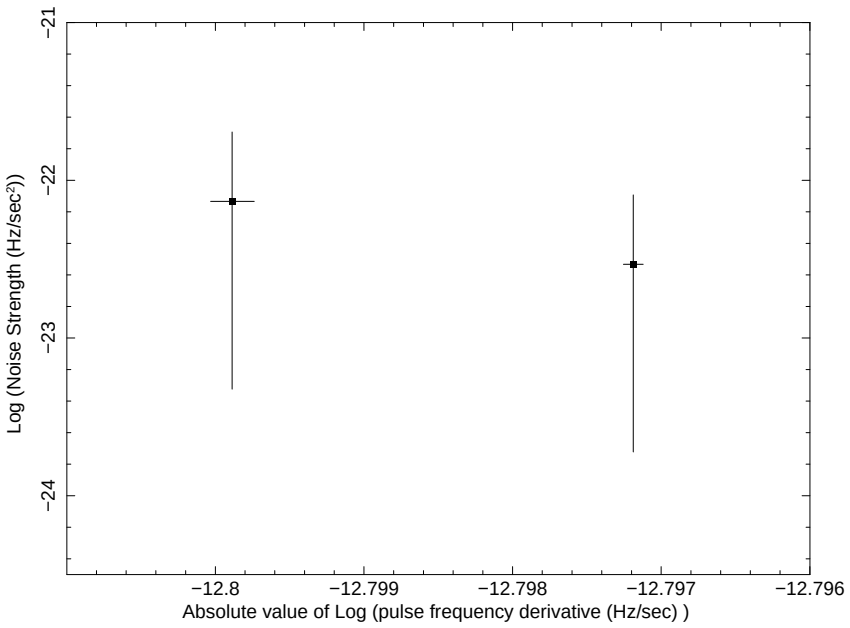

Figure 5.10: Logarithm of timing noise strength as a function of logarithm of absolute value of the spin down rate for 1RXS J170849.0–400910, each point corresponds to the time intervals defined in table 5.6.

Obtained profiles are expressed with harmonic representation and cross-correlated with the master pulse profile. The result of the cross correlation yielded pulse arrivals (figure 5.9). The spin frequency and its derivative is evaluated (see table 5.6). For the Ephemeris F, the calculated timing parameters are marginally different from those of Dib et al. [23], possibly owing to the fact that using high order polynomials leads to a different interpretation of arrivals or it may originate from miscounted cycles. Then the spin-down trend is eliminated from the pulse arrivals to obtain the residuals from which the amplitude of the timing noise is estimated. Then the timing noise strength versus spin-down rate for each interval are plotted (see figure 5.10)

5.4 1E 1841–045

To begin with, the power spectrum of the source from the initial observation set (P40083) is constructed. The pulse frequency at approximately 0.085 Hz and its harmonic can be noticed (see figure 5.11).

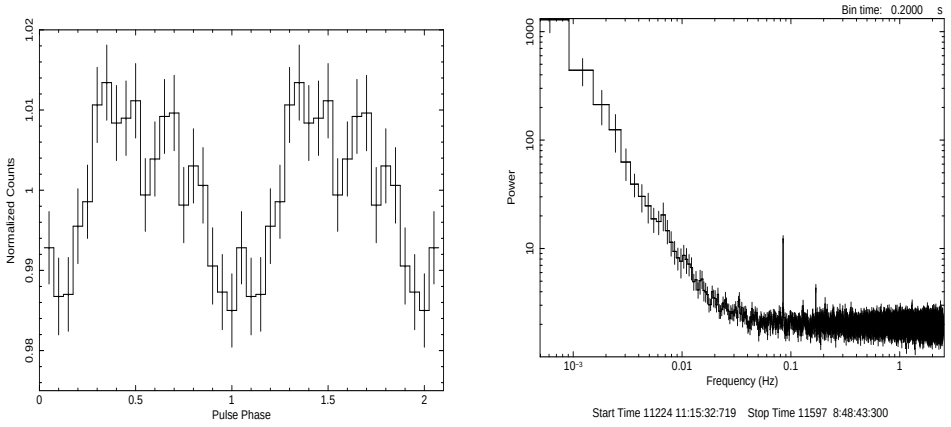

(a) (b)

Figure 5.11: **(a)** Sample pulse profile of 1E 1841–045 obtained, **(b)** Power Spectrum of 1E 1841–045 obtained from *RXTE* observations (observation set P40083). The source signal at ~ 0.085 Hz can be noticed

In 2014, Dib et al. [23] performed an extensive study on the timing characteristics of 1E 1841–045 from August 31, 1996 to December 8, 2011. For the timing analysis, they divided the 16 years of observations to 7 different epochs regarding timing discontinuities. They also calculated a time averaged spin-down rate as -2.95×10^{-13} Hz/s.

Among those time intervals, ephemerises with longer time spans (~ 1000 days), in other words, ephemeris A, C and E are chosen for analysis. We carried out pulse coherent timing method and obtained the pulse arrival times (see figure 5.12).

Associated timing solutions are illustrated in table 5.8. The quadratic trend is removed from pulse arrival times and residuals are obtained. From these residuals, the amplitude of the timing noise is calculated. Then we searched for

Table5.7: Timing Ephemerises of 1E 1841–045

	Start Date (MJD)	End Date (MJD)	Time Span (Days)
Ephemeris A	**51224**	**52437**	**1213**
Ephemeris B1	52481	52773	292
Ephemeris B2	52610	52981	371
Ephemeris C	**53030**	**53815**	**785**
Ephemeris D	53828	54279	451
Ephemeris E	**54307**	**55538**	**1231**
Ephemeris F	55615	55903	288

Notes: Ephemerises given in this table are defined in Dib et al. [23]. Ephemerises written in bold are used in this thesis.

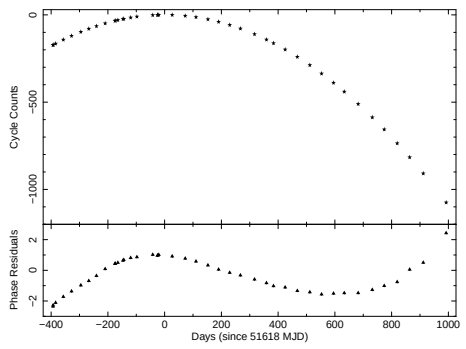

(a)

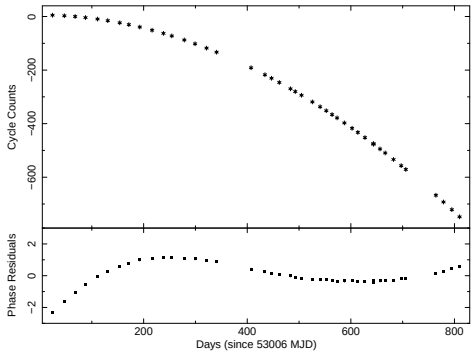

(b)

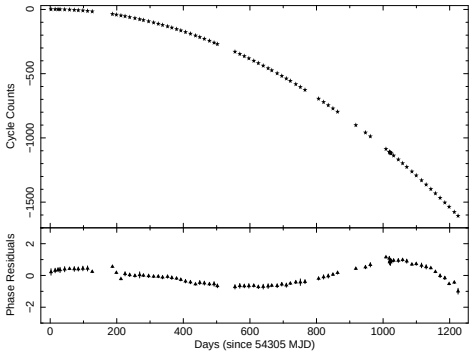

(c)

Figure 5.12: Pulse arrivals and their residuals after removal of spin down trend of 1E 1841–045 for **(a)** Ephemeris A, **(b)** Ephemeris C, **(c)** Ephemeris E.

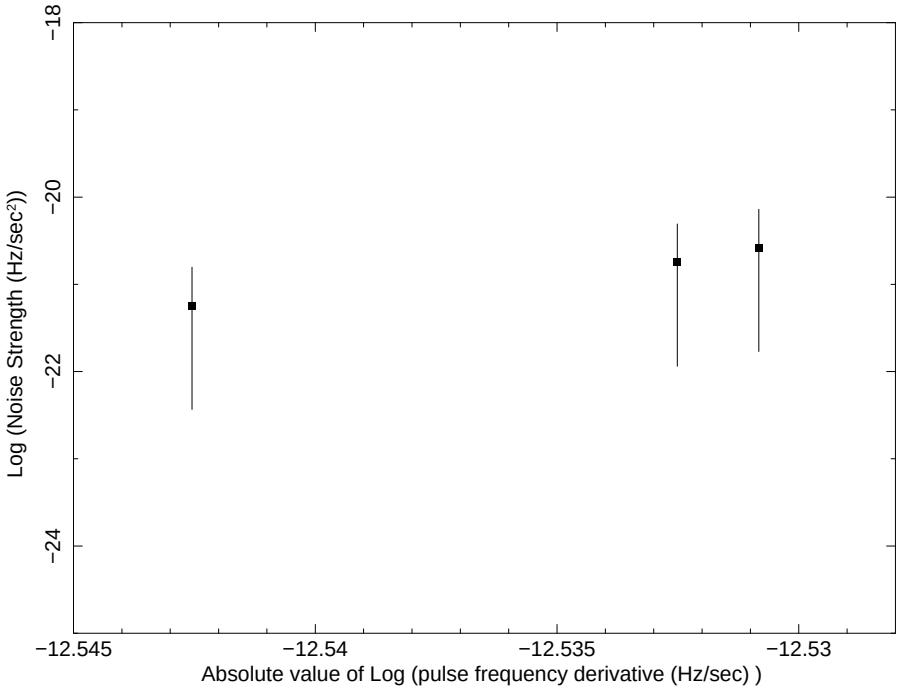

Figure 5.13: Logarithm of timing noise strength as a function of logarithm of absolute value of the spin-down rate for 1E 1841–045, each point corresponds to the time intervals defined in table 5.8. Notice that the uncertainties of spin-down measurements are less then indicative marks.

existence of a correlation between the measured noise strengths and corresponding spin-down rates (see figure 5.13). It is observed that even in the residuals of the same source in different time intervals, noise strength is scaling up with increasing spin down rate.

Table5.8: Timing Parameters of 1E 1841–045

	Epoch (MJD)	Pulse Frequency (Hz)	Spin down rate (10^{-13} Hz/s)
Ephemeris A	**51618.0**	**0.0849253182(5)**	**-2.9342(3)**
Ephemeris A^a	51618.0001	0.0849253010(8)	-2.9954(7)
Ephemeris C	**53006.0**	**0.084889352(17)**	**-2.9456(4)**
Ephemeris C^a	53006.0000	0.084889876(6)	-3.340(7)
Ephemeris E	**54305.0**	**0.084856997(1)**	**-2.8671(1)**
Ephemeris E^a	54305.0000	0.084857001(4)	-2.866(6)

Notes: Superscript **(a)** denotes the timing parameters up to quadratic term obtained by Dib et al. [23]. The ephemerises written in bold represents the results of this study.

CHAPTER 6

DISCUSSION AND CONCLUSION

6.1 Discussion

Existence of a correlation between spin down rate and timing noise strength was previously illustrated for radio pulsars ((Cordes & Helfand [17]; Arzoumanian et al. [4]). Similar type of a correlation for magnetars are also discussed by (Woods et al. [93]; Gavriil & Kaspi [36], Serim et al. [78]). Gavriil & Kaspi [36]

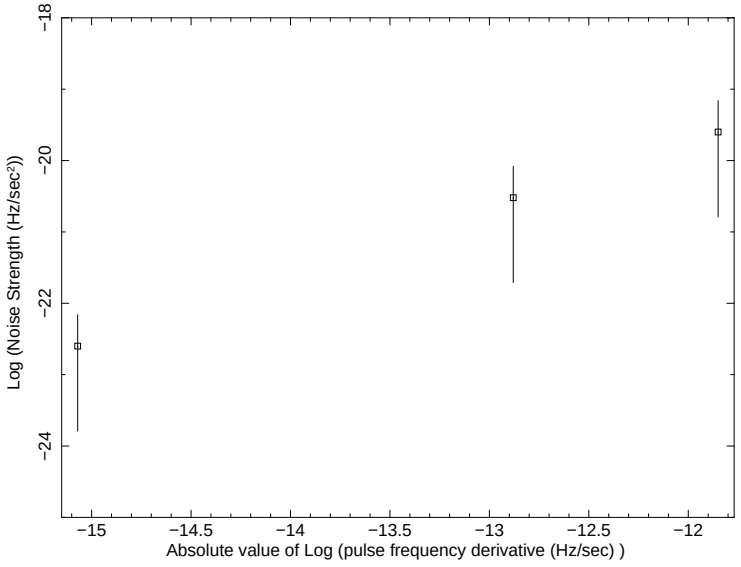

Figure 6.1: Logarithm of timing noise strength as a function of logarithm of absolute value of the spin-down rate for 3 SGRs: SGR 1833–0832, SWIFT J1822.3–1606 and SWIFT J1834.9–0846[1]

claimed that such correlation may exist for all of them (i.e. both pulsars and magnetars), however; observed burst of these sources seem to be occurring after a threshold for both timing noise strength and spin down rate. Serim et al. [78] considered three SGRs in particular (SGR 1833–0832, Swift J1822.3–1606 and Swift J1834.9–0846), and estimated the noise strengths of these objects. Their data spans rather short time intervals ranging from $\sim 150 - 250$ days. They claimed that there is a possible correlation between frequency derivative and estimated timing noise strength of these objects (see figure 6.1).

In 1972, Boynton et al. [10] discussed possible mechanisms that can producered noise in spin-down rate, (i.e. random walks in frequency) and stated that one of the possible mechanism is crust cracking. In this model, the moment of inertia of the pulsar can change due to micro-cracks on the crust of the neutron stars. Another mechanism is put forward by Rudermann et al. [76] which explains the crustal tectonic motions as a generator of such noise. In both cases, cracking of

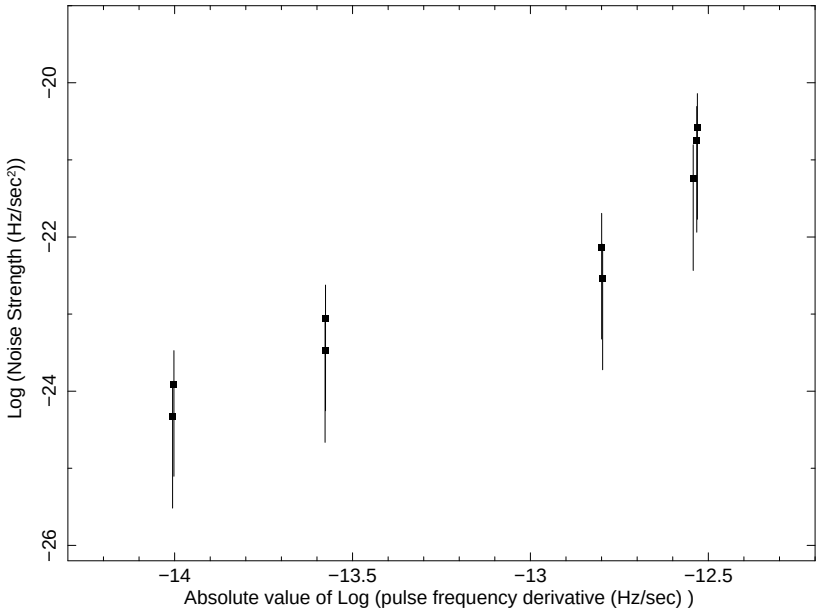

Figure 6.2: Logarithm of timing noise strength as a function of logarithm of absolute value of the spin down rate for 4 AXPs: 4U 0142+61, 1E 2259+586, 1RXS J170849.0–400910 and 1E 1841–045

[1]adapted from [78]

crust causes a change in the moment of inertia of the magnetar, and produce the timing noise we observe from these sources.

Another possibility discussed by Tsang and Gourgouliatos [86] is magnetospherical moment of inertia variations. They suggested that variability should be taking place near the neutron star surface rather than light cylinder. They concluded that rapid global magnetospheric variations (such as magnetic reconnection) should be the source of the timing noise. The red noise in spin down rate may also be originated from external torques from the magnetosphere (e.g pair production) [16] which is shown to be in agreement with the observations of several pulsars [6].

In this thesis, the timing noise of four AXPs are investigated in detail, and it is observed that timing noise strength of these objects are also scaling up with

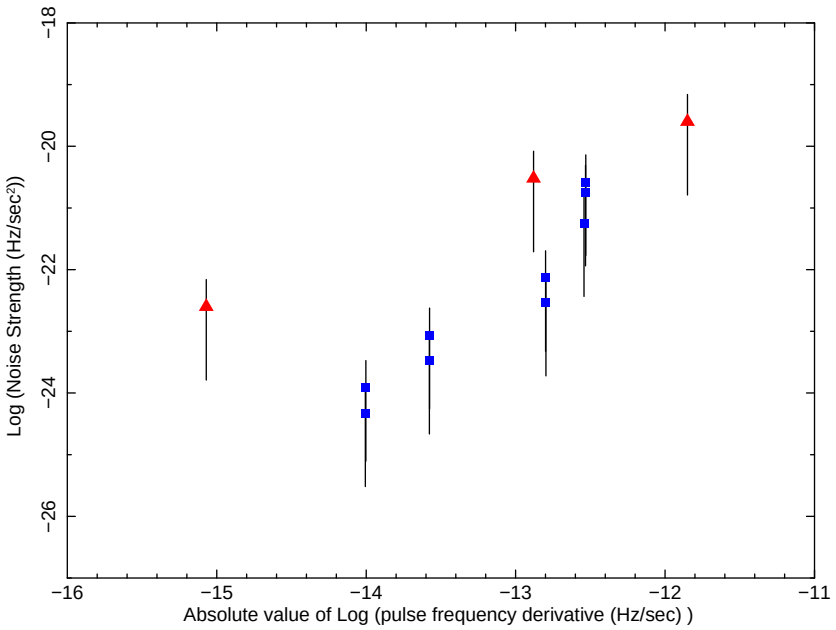

Figure 6.3: Logarithm of timing noise strength as a function of logarithm of absolute value of the spin down rate for 4 AXPs (blue squares) and 3 SGRs[2](red triangles): 4U 0142+61, 1E 2259+586, 1RXS J170849.0–400910, 1E 1841–045, SGR 1833–0832, SWIFT J1822.3–1606 and SWIFT J1834.9–0846.

[2]values are obtained from [78]

the increasing spin down as it is claimed by Serim et al. [78] for SGRs. It is rather remarkable to notice that same trend can be seen within two of AXPs (1E 2259+586 and 1E 1841–045) while the trend is absent in the other two AXPs (4U 0142+61 and 1RXS J170849.0–400910) (see chapter 5 for details). In addition, when these four AXPs are put together in one, it can also be seen that the correlation also holds for selected AXPs (see figure 6.2).

As the AXPs and SGRs belong to same class, that is magnetars, the correlation as whole class should also be taken into account. Even though, the noise strength is scaling up in both cases, it seems that they rather have their own correlations rather than a overall correlation for magnetars (see figure 6.3). And SGRs seem to possess more timing noise than AXPs. However; the difference might be originated from the fact that the time scales used for calculation of noise strength of SGRs by Serim et al. [78] are relatively short. But in both cases, this noise correlation can be interpreted as micro-scale cracks in neutron stars crust [10]. The high magnetic field of magnetars generate great stress in the crust, which would lead to small amplitude cracks. The existence of such cracks may alter the moment of inertia in very small amounts, and that is to be associated with the torque. Hence, torque changes yield modulation in spin-down rate of the magnetar.

6.2 Conclusion

The analysis carried out in thesis aimed to reveal timing noise of magnetars and the associated physics behind it. Hence, timing characteristics of four AXPs; 4U 0142+61, 1E 2259+586, 1RXS J170849.0–400910, and 1E 1841–045 are investigated. The timing parameters are calculated for "glitch free" time intervals with relatively long time spans ($\sim$ 1000 days). After obtaining timing parameters, residuals of spin-down trends are extracted for each time interval for every source. Then, the noise strength of each interval is calculated separately in order to see if spin-down and timing noise strength correlates;
i) for same source in different time intervals (i.e. different spin-down rates)
ii) for the selected four AXPs in overall.
iii) for the 7 magnetars in overall (3 SGRs and 4 AXPs).
For the case **i**, even though timing noise strength seem to correlate with the spin-down rate for 1E 2259+586 and 1E 1841–045, there is no clear pattern in other 2 AXPs (4U 0142+61 and 1RXS J170849.0–400910). In additon, it should be noted that uncertainties in the noise strength measurements do not allow to resolve the correlation pattern (if there are any). Case **ii** was previously studied for SGRs,and it was suggested that there may exist a correlation between frequency derivative and noise strength [78]. Our preliminary results leads to an interpretation that timing noise strength is scaling up with the increasing frequency derivative for four AXPs as well. However, case **iii** requires noise strength estimations from all possible magnetars to achieve more consistent results. Also, the time intervals should be approximately similar in length to have a better comparison.

But we conclude that the feasible model to produce such timing noise is crust cracking [10]. With such mechanism, small amplitude cracks can afford to explain the increase of timing noise with increasing spin down rate.

REFERENCES

[1] M. A. Alpar. On Young Neutron Stars as Propellers and Accretors with Conventional Magnetic Fields. *Astrophysical Journal*, 554:1245–1254, June 2001.

[2] M. A. Alpar. On kHz oscillations and characteristic frequencies of accreting magnetospheres. *Monthly Notices of the Royal Astronomical Society*, 423:3768–3774, July 2012.

[3] R. F. Archibald, V. M. Kaspi, C.-Y. Ng, K. N. Gourgouliatos, D. Tsang, P. Scholz, A. P. Beardmore, N. Gehrels, and J. A. Kennea. An anti-glitch in a magnetar. *Nature*, 497:591–593, May 2013.

[4] Z. Arzoumanian, D. J. Nice, J. H. Taylor, and S. E. Thorsett. Timing behavior of 96 radio pulsars. *Astrophysical Journal*, 422:671–680, Feb. 1994.

[5] W. Baade and F. Zwicky. Cosmic Rays from Super-novae. *Contributions from the Mount Wilson Observatory, vol. 3, pp.79-83*, 3:79–83, 1934.

[6] A. Baykal, M. Ali Alpar, P. E. Boynton, and J. E. Deeter. The timing noise of PSR 0823+26,1706-16, 1749-28, 2021+51 and the anomalous brakingindices. *Monthly Notices of the Royal Astronomical Society*, 306:207–212, June 1999.

[7] A. Baykal, J. H. Swank, T. Strohmayer, and M. J. Stark. Spin-down rate of 1E 2259+586 from RXTE observation. *Astronomy and Astrophysics*, 336:173–176, Aug. 1998.

[8] A. M. Beloborodov and C. Thompson. Corona of Magnetars. *Astrophysical Journal*, 657:967–993, Mar. 2007.

[9] G. F. Bignami, P. A. Caraveo, A. De Luca, and S. Mereghetti. Discovery of X-ray cyclotron absorption lines measures the magnetic field of an isolated neutron star. *ArXiv Astrophysics e-prints*, June 2003.

[10] P. E. Boynton, E. J. Groth, D. P. Hutchinson, G. P. Nanos, Jr., R. B. Partridge, and D. T. Wilkinson. Optical Timing of the Crab Pulsar, NP 0532. *Astrophysical Journal*, 175:217, July 1972.

[11] H. V. Bradt, R. E. Rothschild, and J. H. Swank. X-ray timing explorer mission. *Astronomy and Astrophysics, Supplement*, 97:355–360, Jan. 1993.

[12] S. Şaşmaz Muş and E. Göğüş. Long-term Timing and Glitch Characteristics of Anomalous X-Ray Pulsar 1RXS J170849.0-400910. *Astrophysical Journal*, 778:156, Dec. 2013.

[13] S. Campana, N. Rea, G. L. Israel, R. Turolla, and S. Zane. Swift and Chandra confirm the intensity-hardness correlation of the AXP 1RXS J170849.0-400910. *Astronomy and Astrophysics*, 463:1047–1051, Mar. 2007.

[14] D. Chakrabarty, Z. Wang, and D. L. Kaplan. A debris disk around an isolated young neutron star. In *36th COSPAR Scientific Assembly*, volume 36 of *COSPAR Meeting*, page 1504, 2006.

[15] P. Chatterjee, L. Hernquist, and R. Narayan. An Accretion Model for Anomalous X-Ray Pulsars. *Astrophysical Journal*, 534:373–379, May 2000.

[16] K. S. Cheng. Could glitches inducing magnetospheric fluctuations produce low-frequency pulsar timing noise? *Astrophysical Journal*, 321:805–812, Oct. 1987.

[17] J. M. Cordes and D. J. Helfand. Pulsar timing. III - Timing noise of 50 pulsars. *Astrophysical Journal*, 239:640–650, July 1980.

[18] S. Dall'Osso, G. L. Israel, L. Stella, A. Possenti, and E. Perozzi. The Glitches of the Anomalous X-Ray Pulsar 1RXS J170849.0-400910. *Astrophysical Journal*, 599:485–497, Dec. 2003.

[19] J. E. Deeter. Techniques for the estimation of red power spectra. II Evaluation of alternative methods. *Astrophysical Journal*, 281:482–491, June 1984.

[20] J. E. Deeter and P. E. Boynton. Techniques for the estimation of red power spectra. I - Context and methodology. *Astrophysical Journal*, 261:337–350, Oct. 1982.

[21] P. R. den Hartog, L. Kuiper, W. Hermsen, V. M. Kaspi, R. Dib, J. Knödlseder, and F. P. Gavriil. Detailed high-energy characteristics of AXP 4U 0142+61. Multi-year observations with INTEGRAL, RXTE, XMM-Newton, and ASCA. *Astronomy and Astrophysics*, 489:245–261, Oct. 2008.

[22] R. Dib. *RXTE monitoring of 5 anomalous x-ray pulsars.* PhD thesis, McGill University, Canada, 2009.

[23] R. Dib and V. M. Kaspi. 16 yr of RXTE Monitoring of Five Anomalous X-Ray Pulsars. *Astrophysical Journal*, 784:37, Mar. 2014.

[24] R. Dib, V. M. Kaspi, and F. P. Gavriil. 10 Years of RXTE Monitoring of the Anomalous X-Ray Pulsar 4U 0142+61: Long-Term Variability. *Astrophysical Journal*, 666:1152–1164, Sept. 2007.

[25] R. Dib, V. M. Kaspi, and F. P. Gavriil. Glitches in Anomalous X-Ray Pulsars. *Astrophysical Journal*, 673:1044–1061, Feb. 2008.

[26] R. C. Duncan. Magnetar Models for Soft Gamma Repeaters and Anomalous X-ray Pulsars. In *American Astronomical Society Meeting Abstracts*, volume 30 of *Bulletin of the American Astronomical Society*, page 1332, Dec. 1998.

[27] R. C. Duncan and C. Thompson. Formation of very strongly magnetized neutron stars - Implications for gamma-ray bursts. *Astrophysical Journal, Letters*, 392:L9–L13, June 1992.

[28] M. Durant and M. H. van Kerkwijk. Multiwavelength Variability of the Magnetar 4U 0142+61. *Astrophysical Journal*, 652:576–583, Nov. 2006.

[29] M. Durant and M. H. van Kerkwijk. The Infrared Counterpart to the Magnetar 1RXS J170849.0-400910. *Astrophysical Journal*, 648:534–540, Sept. 2006.

[30] C. M. Espinoza, A. G. Lyne, M. Kramer, R. N. Manchester, and V. M. Kaspi. The Braking Index of PSR J1734-3333 and the Magnetar Population. *Astrophysical Journal, Letters*, 741:L13, Nov. 2011.

[31] D. Evans, R. Kiebesadel, J. Baros, T. Cline, U. Desai, B. Teegarden, G. Pizzichini, K. Hurley, M. Niel, G. Vedrenne, I. V. Estulin, and E. P. Mazets. Gamma-ray Burst 79-03-05. *IAU Cirulars*, 3356:1, May 1979.

[32] G. G. Fahlman and P. C. Gregory. An X-ray pulsar in SNR G109.1-1.0. *Nature*, 293:202–204, Sept. 1981.

[33] G. G. Fahlman and P. C. Gregory. The Discovery of an X-Ray Pulsar in the SNR G109.1-1.0. In *Bulletin of the American Astronomical Society*, volume 13 of *Bulletin of the American Astronomical Society*, page 533, Mar. 1981.

[34] W. Forman, C. Jones, L. Cominsky, P. Julien, S. Murray, G. Peters, H. Tananbaum, and R. Giacconi. The fourth Uhuru catalog of X-ray sources. *Astrophysical Journal, Supplement*, 38:357–412, Dec. 1978.

[35] F. P. Gavriil, R. Dib, and V. M. Kaspi. The 2006-2007 Active Phase of Anomalous X-ray Pulsar 4U 0142+61: Radiative and Timing Changes, Bursts, and Burst Spectral Features. *Astrophysical Journal*, 736:138, Aug. 2011.

[36] F. P. Gavriil and V. M. Kaspi. Long-Term Rossi X-Ray Timing Explorer Monitoring of Anomalous X-Ray Pulsars. *Astrophysical Journal*, 567:1067–1076, Mar. 2002.

[37] F. P. Gavriil, V. M. Kaspi, and P. M. Woods. Magnetar-like X-ray bursts from an anomalous X-ray pulsar. *Nature*, 419:142–144, Sept. 2002.

[38] F. P. Gavriil, V. M. Kaspi, and P. M. Woods. A Comprehensive Study of the X-Ray Bursts from the Magnetar Candidate 1E 2259+586. *Astrophysical Journal*, 607:959–969, June 2004.

[39] E. V. Gotthelf. An Ultra-Magnetized X-ray Pulsar in the Supernova Remnant KES 73. *News Letter of the Astronomical Society of New York*, 5:22, Aug. 1999.

[40] D. Götz, N. Rea, G. L. Israel, S. Zane, P. Esposito, E. V. Gotthelf, S. Mereghetti, A. Tiengo, and R. Turolla. Long term hard X-ray variability of the anomalous X-ray pulsar 1RXS J170849.0-400910 discovered with INTEGRAL. *Astronomy and Astrophysics*, 475:317–321, Nov. 2007.

[41] P. C. Gregory and G. G. Fahlman. An extraordinary new celestial X-ray source. *Nature*, 287:805, Oct. 1980.

[42] A. Hewish, S. J. Bell, J. D. H. Pilkington, P. F. Scott, and R. A. Collins. Observation of a Rapidly Pulsating Radio Source. *Nature*, 217:709–713, Feb. 1968.

[43] J. Hjorth, J. Sollerman, P. Møller, J. P. U. Fynbo, S. E. Woosley, C. Kouveliotou, N. R. Tanvir, J. Greiner, M. I. Andersen, A. J. Castro-Tirado, J. M. Castro Cerón, A. S. Fruchter, J. Gorosabel, P. Jakobsson, L. Kaper, S. Klose, N. Masetti, H. Pedersen, K. Pedersen, E. Pian, E. Palazzi, J. E. Rhoads, E. Rol, E. P. J. van den Heuvel, P. M. Vreeswijk, D. Watson, and R. A. M. J. Wijers. A very energetic supernova associated with the γ-ray burst of 29 March 2003. *Nature*, 423:847–850, June 2003.

[44] V. A. Hughes, R. H. Harten, and S. van den Bergh. A new supernova remnant G109.2-1.0. *Astrophysical Journal, Letters*, 246:L127–L131, June 1981.

[45] B. Içdem, A. Baykal, and S. Ç. Inam. RXTE timing analysis of the anomalous X-ray pulsar 1E 2259+586. *Monthly Notices of the Royal Astronomical Society*, 419:3109–3114, Feb. 2012.

[46] G. Israel, T. Oosterbroek, L. Stella, S. Campana, S. Mereghetti, and A. N. Parmar. The Pulse-Phase-dependent Spectrum of the Anomalous X-Ray Pulsar 1RXS J170849-400910. *Astrophysical Journal, Letters*, 560:L65–L69, Oct. 2001.

[47] G. L. Israel, S. Covino, L. Stella, S. Campana, F. Haberl, and S. Mereghetti. Further Evidence that 1RXS J170849.0-400910 Is an Anomalous X-Ray Pulsar. *Astrophysical Journal, Letters*, 518:L107–L110, June 1999.

[48] G. L. Israel, D. Götz, S. Zane, S. Dall'Osso, N. Rea, and L. Stella. Linking the X-ray timing and spectral properties of the glitching AXP 1RXS J170849-400910. *Astronomy and Astrophysics*, 476:L9–L12, Dec. 2007.

[49] G. L. Israel, S. Mereghetti, and L. Stella. The discovery of 8.7 second pulsations from the ultrasoft X-ray source 4U 0142+61. *Astrophysical Journall*, 433:L25–L28, Sept. 1994.

[50] K. Jahoda, J. H. Swank, A. B. Giles, M. J. Stark, T. Strohmayer, W. Zhang, and E. H. Morgan. In-orbit performance and calibration of the Rossi X-ray Timing Explorer (RXTE) Proportional Counter Array (PCA). In O. H. Siegmund and M. A. Gummin, editors, *EUV, X-Ray, and Gamma-Ray Instrumentation for Astronomy VII*, volume 2808 of *Society of Photo-Optical Instrumentation Engineers (SPIE) Conference Series*, pages 59–70, Oct. 1996.

[51] V. Kaspi. Magnetars in Perspective. In *40th COSPAR Scientific Assembly. Held 2-10 August 2014, in Moscow, Russia, Abstract E1.12-1-14.*, volume 40 of *COSPAR Meeting*, page 1416, 2014.

[52] V. M. Kaspi, D. Chakrabarty, and J. Steinberger. Precision Timing of Two Anomalous X-Ray Pulsars. *Astrophysical Journall*, 525:L33–L36, Nov. 1999.

[53] V. M. Kaspi and F. P. Gavriil. A Second Glitch from the "Anomalous" X-Ray Pulsar 1RXS J170849.0-4000910. *Astrophysical Journal, Letters*, 596:L71–L74, Oct. 2003.

[54] V. M. Kaspi, F. P. Gavriil, P. M. Woods, J. B. Jensen, M. S. E. Roberts, and D. Chakrabarty. A Major Soft Gamma Repeater-like Outburst and Rotation Glitch in the No-longer-so-anomalous X-Ray Pulsar 1E 2259+586. *Astrophysical Journal, Letters*, 588:L93–L96, May 2003.

[55] V. M. Kaspi, J. R. Lackey, and D. Chakrabarty. A Glitch in an Anomalous X-Ray Pulsar. *Astrophysical Journal, Letters*, 537:L31–L34, July 2000.

[56] C. Kouveliotou, M. Kippen, P. Woods, G. Richardson, and V. Connaughton. Discovery of a new Sgr source, SGR1627-41. *GRB Coordinates Network*, 107:1, 1998.

[57] G. A. Kriss and C. R. Canizares. X-ray properties of quasars and results from a deep X-ray survey of optically selected objects. *Astrophysical Journal*, 297:177–193, Oct. 1985.

[58] L. Kuiper, W. Hermsen, P. R. den Hartog, and W. Collmar. Discovery of Luminous Pulsed Hard X-Ray Emission from Anomalous X-Ray Pulsars 1RXS J1708-4009, 4U 0142+61, and 1E 2259+586 by INTEGRAL and RXTE. *Astrophysical Journal*, 645:556–575, July 2006.

[59] L. Kuiper, W. Hermsen, and M. Mendez. Discovery of Hard Nonthermal Pulsed X-Ray Emission from the Anomalous X-Ray Pulsar 1E 1841-045. *Astrophysical Journal*, 613:1173–1178, Oct. 2004.

[60] H. S. Kumar and S. Safi-Harb. Swift Study of the First Soft γ-ray Repeater Like Burst from AXP 1E 1841-045 in SNR Kes 73. *Astrophysical Journal, Letters*, 725:L191–L195, Dec. 2010.

[61] J. M. Lattimer and M. Prakash. Neutron Star Structure and the Equation of State. *Astrophysical Journal*, 550:426–442, Mar. 2001.

[62] L. Lin, C. Kouveliotou, E. Göğüş, A. J. van der Horst, A. L. Watts, M. G. Baring, Y. Kaneko, R. A. M. J. Wijers, P. M. Woods, S. Barthelmy, J. M. Burgess, V. Chaplin, N. Gehrels, A. Goldstein, J. Granot, S. Guiriec, J. Mcenery, R. D. Preece, D. Tierney, M. van der Klis, A. von Kienlin, and S. N. Zhang. Burst and Persistent Emission Properties during the Recent Active Episode of the Anomalous X-Ray Pulsar 1E 1841-045. *Astrophysical Journal, Letters*, 740:L16, Oct. 2011.

[63] E. P. Mazets and S. V. Golenetskii. Recent results from the gamma-ray burst studies in the KONUS experiment. *Astrophysics and Space Science*, 75:47–81, Mar. 1981.

[64] E. P. Mazets, S. V. Golenetskij, and Y. A. Guryan. Soft gamma-ray bursts from the source B1900+14. *Soviet Astronomy Letters*, 5:343, Dec. 1979.

[65] S. Mereghetti. The strongest cosmic magnets: soft gamma-ray repeaters and anomalous X-ray pulsars. *Astronomy and Astrophysics Reviews*, 15:225–287, July 2008.

[66] S. Mereghetti, G. L. Israel, and L. Stella. New limits on the orbital parameters of 1E 1048.1-5937 and 1E 2259+586 from RXTE observations. *Monthly Notices of the Royal Astronomical Society*, 296:689–692, May 1998.

[67] S. Mereghetti and L. Stella. The very low mass X-ray binary pulsars: A new class of sources? *Astrophysical Journal, Letters*, 442:L17–L20, Mar. 1995.

[68] S. V. Molkov, A. M. Cherepashchuk, A. A. Lutovinov, M. G. Revnivtsev, K. A. Postnov, and R. A. Sunyaev. A Hard X-ray Survey of the Sagittarius Arm Tangent with the IBIS Telescope of the INTEGRAL Observatory: A Catalog of Sources. *Astronomy Letters*, 30:534–539, Aug. 2004.

[69] M. Morini, N. R. Robba, A. Smith, and M. van der Klis. EXOSAT observations of the supernova remnant G109.1-1.0 and the X-ray pulsar 1E 2259+586. *Astrophysical Journal*, 333:777–787, Oct. 1988.

[70] S. A. Olausen and V. M. Kaspi. The McGill Magnetar Catalog. *Astrophysical Journal, Supplement*, 212:6, May 2014.

[71] B. Paczynski. Gamma-Ray Bursts: Facts and Fantasies. In *American Astronomical Society Meeting Abstracts #180*, volume 24 of *Bulletin of the American Astronomical Society*, page 751, May 1992.

[72] P. A. Price, E. Berger, D. E. Reichart, S. R. Kulkarni, S. A. Yost, R. Subrahmanyan, R. M. Wark, M. H. Wieringa, D. A. Frail, J. Bailey, B. Boyle, E. Corbett, K. Gunn, S. D. Ryder, N. Seymour, K. Koviak, P. McCarthy, M. Phillips, T. S. Axelrod, J. S. Bloom, S. G. Djorgovski, D. W. Fox, T. J. Galama, F. A. Harrison, K. Hurley, R. Sari, B. P. Schmidt, M. J. I. Brown, T. Cline, F. Frontera, C. Guidorzi, and E. Montanari. GRB 011121: A Massive Star Progenitor. *Astrophysical Journal, Letters*, 572:L51–L55, June 2002.

[73] N. Rea, P. Esposito, R. Turolla, G. L. Israel, S. Zane, L. Stella, S. Mereghetti, A. Tiengo, D. Götz, E. Göğüş, and C. Kouveliotou. A Low-Magnetic-Field Soft Gamma Repeater. *Science*, 330:944–, Nov. 2010.

[74] N. Rea, T. Oosterbroek, S. Zane, R. Turolla, M. Méndez, G. L. Israel, L. Stella, and F. Haberl. Post-glitch variability in the anomalous X-ray pulsar 1RXSJ170849.0-400910. *Monthly Notices of the Royal Astronomical Society*, 361:710–718, Aug. 2005.

[75] N. Rea, R. Turolla, S. Zane, A. Tramacere, L. Stella, G. L. Israel, and R. Campana. Spectral Modeling of the High-Energy Emission of the Magnetar 4U 0142+614. *Astrophysical Journal, Letters*, 661:L65–L68, May 2007.

[76] R. Ruderman. Neutron star crustal plate tectonics. II - Evolution of radio pulsar magnetic fields. III - Cracking, glitches, and gamma-ray bursts. *Astrophysical Journal*, 382:576–593, Dec. 1991.

[77] P. Scholz, R. F. Archibald, V. M. Kaspi, C.-Y. Ng, A. P. Beardmore, N. Gehrels, and J. A. Kennea. On the X-Ray Variability of Magnetar 1RXS J170849.0-400910. *Astrophysical Journal*, 783:99, Mar. 2014.

[78] M. M. Serim, S. Ç. Inam, and A. Baykal. Noise Strength Estimates of Three SGRs: Swift J1822.3-1606, SGR J1833-0832 and Swift J1834.9-0846. In W. Lewandowski, O. Maron, and J. Kijak, editors, *Electromagnetic Radiation from Pulsars and Magnetars*, volume 466 of *Astronomical Society of the Pacific Conference Series*, page 255, Dec. 2012.

[79] F. D. Seward, P. A. Charles, and A. P. Smale. A 6 second periodic X-ray source in Carina. *Astrophysical Journal*, 305:814–816, June 1986.

[80] J. H. Swank, K. Jahoda, W. Zhang, A. B. Giles, F. M. Marshall, H. V. Bradt, A. M. Levine, E. H. Morgan, R. A. Remillard, R. E. Rothschild, D. E. Gruber, P. L. Hink, and M. R. Pelling. The X-ray Timing Explorer: Progress and Science Prospects. In M. A. Alpar, U. Kiziloglu, and J. van Paradijs, editors, *NATO Advanced Science Institutes (ASI) Series C*, volume 450 of *NATO Advanced Science Institutes (ASI) Series C*, page 525, 1995.

[81] C. Thompson and R. C. Duncan. The soft gamma repeaters as very strongly magnetized neutron stars - I. Radiative mechanism for outbursts. *Monthly Notices of the Royal Astronomical Society*, 275:255–300, July 1995.

[82] C. Thompson and R. C. Duncan. The Soft Gamma Repeaters as Very Strongly Magnetized Neutron Stars. II. Quiescent Neutrino, X-Ray, and Alfven Wave Emission. *Astrophysical Journal*, 473:322, Dec. 1996.

[83] C. Thompson and R. C. Duncan. The Giant Flare of 1998 August 27 from SGR 1900+14. II. Radiative Mechanism and Physical Constraints on the Source. *Astrophysical Journal*, 561:980–1005, Nov. 2001.

[84] W. W. Tian and D. A. Leahy. The Distance and Age of the Supernova Remnants Kes 73 and AXP 1E 1841-045. *Astrophysical Journal*, 677:292–296, Apr. 2008.

[85] W. W. Tian, D. A. Leahy, and D. Li. Distance to the SNR CTB109/AXP1E2259+586 by HI absorption and self-absorption. *Monthly Notices of the Royal Astronomical Society*, 404:L1–L5, May 2010.

[86] D. Tsang and K. N. Gourgouliatos. Timing Noise in Pulsars and Magnetars and the Magnetospheric Moment of Inertia. *Astrophysical Journal, Letters*, 773:L17, Aug. 2013.

[87] M. van der Klis. Fourier techniques in X-ray timing. In H. Ögelman and E. P. J. van den Heuvel, editors, *NATO Advanced Science Institutes (ASI) Series C*, volume 262 of *NATO Advanced Science Institutes (ASI) Series C*, page 27, 1989.

[88] J. van Paradijs, R. E. Taam, and E. P. J. van den Heuvel. On the nature of the 'anomalous' 6-s X-ray pulsars. *Astronomy and Astrophysics*, 299:L41, July 1995.

[89] G. Vasisht and E. V. Gotthelf. The Discovery of an Anomalous X-Ray Pulsar in the Supernova Remnant Kes 73. *Astrophysical Journal, Letters*, 486:L129–L132, Sept. 1997.

[90] W. Voges, T. Boller, K. Dennerl, J. Englhauser, R. Gruber, F. Haberl, J. Paul, W. Pietsch, J. Trümper, and H. U. Zimmermann. Identification of

the ROSAT All-Sky Survey sources. In H. U. Zimmermann, J. Trümper, and H. Yorke, editors, *Roentgenstrahlung from the Universe*, pages 637–640, Feb. 1996.

[91] Z. Wang, D. Chakrabarty, and D. L. Kaplan. A debris disk around an isolated young neutron star. *Nature*, 440:772–775, Apr. 2006.

[92] P. M. Woods, V. M. Kaspi, C. Thompson, F. P. Gavriil, H. L. Marshall, D. Chakrabarty, K. Flanagan, J. Heyl, and L. Hernquist. Changes in the X-Ray Emission from the Magnetar Candidate 1E 2259+586 during Its 2002 Outburst. *Astrophysical Journal*, 605:378–399, Apr. 2004.

[93] P. M. Woods, C. Kouveliotou, M. H. Finger, E. Göğüş, D. M. Scott, S. Dieters, C. Thompson, R. C. Duncan, K. Hurley, T. Strohmayer, J. Swank, and T. Murakami. Timing Noise in SGR 1806-20. *Astrophysical Journal, Letters*, 535:L55–L58, May 2000.

[94] P. M. Woods and C. Thompson. *Soft gamma repeaters and anomalous X-ray pulsars: magnetar candidates*, pages 547–586. Apr. 2006.

[95] W. Zhu, V. M. Kaspi, R. Dib, P. M. Woods, F. P. Gavriil, and A. M. Archibald. The Long-term Radiative Evolution of Anomalous X-Ray Pulsar 1E 2259+586 After its 2002 Outburst. *Astrophysical Journal*, 686:520–527, Oct. 2008.